Chapter 3

Small Signal Modelling

The previous chapter gives the existing background in literature for the research work carried out in this thesis. This chapter focusses on the small signal analysis of the microgrid system while obtaining the state space representations of complex AC microgrid system and DC microgrid system. The detailed mathematical formulation of these systems with the transfer function modelling has been analysed. The chapter also includes simulation results obtained in MATLAB 2016a environment for the small signal modelling with certain state perturbations.

3.1 Preliminaries

Some of the preliminaries to small signal modelling of AC and DC microgrid systems in both autonomous and grid-tied mode have been discussed in this section.

3.1.1 Reference frames

The mathematical modelling in power system analysis has been greatly simplified with the transformation theory wherein the dependent variables can be decoupled for solving time-varying complex electrical equations[75]. The three commonly used reference frames are:

- Three phase reference frame (*ABC-Frame*): The three axis are coplanar and at 120 degree from each other.

- Two phase stationary reference frame (*αβ-Frame*): Two axis are coplanar and perpendicular(orthogonal) to each other.
- Two phase synchronous reference frame (*dq-Frame*): d-axis is at θ degree(rotating angle) to α axis and q-axis is perpendicular to d-axis.

Among the various transformations available, the most commonly used are; Park Transformation and Clarke Transformation [77]. Mathematical interpretations of these transformations has been discussed below.

Park Transformation

The two axis orthogonal stationary reference frame quantities are transformed to two axis ortogonal rotating reference frame by Park Transformation.

$$x_d = x_\alpha \cos\theta + x_\beta \sin\theta$$

$$x_q = x_\beta \cos\theta - x_\alpha \sin\theta \quad (3.1)$$

where, $x_{dq}$is the rotating two phase quantity and $x_{\alpha\beta}$ is the stationary two phase quantity. θ is the rotating angle.

$$[dq] = \begin{bmatrix} \cos\theta & \sin\theta \\ -\sin\theta & \cos\theta \end{bmatrix} [\alpha\beta] \quad (3.2)$$

Where $\begin{bmatrix} \cos\theta & \sin\theta \\ -\sin\theta & \cos\theta \end{bmatrix}$is called the *Park matrix*.

Clarke Transformation

The three phase quantities are transformed from three phase reference frame to two phase stationary orthogonal reference frame by Clarke Transformation.

$$x_\alpha = \frac{2}{3}x_a - \frac{1}{3}(x_b - x_c)$$

$$x_\beta = \frac{2}{\sqrt{3}}(x_b - x_c) \quad (3.3)$$

where, $x_{abc}$is the three phase quantity and $x_{\alpha\beta}$ is the two phase orthogonal quantity.

$$[\alpha\beta] = \frac{2}{3} \times \begin{bmatrix} 1 & -1/2 & -1/2 \\ 0 & \sqrt{3}/2 & -\sqrt{3}/2 \end{bmatrix} [abc] \tag{3.4}$$

where $\frac{2}{3} \times \begin{bmatrix} 1 & -1/2 & -1/2 \\ 0 & \sqrt{3}/2 & -\sqrt{3}/2 \end{bmatrix}$ is called the *Clarke matrix*.

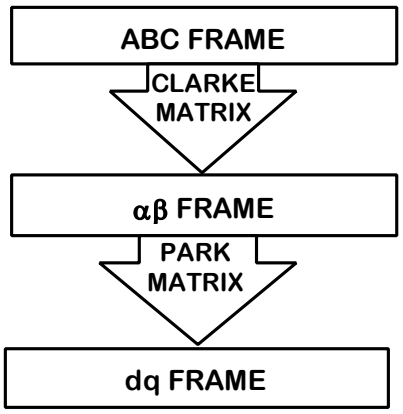

Figure 3.1. *Frame transformation*

The inter-conversion between the three reference frames as in Figure 3.1. is self-explanatory [77]. Further, the transformation of three phase quantities from ABC frame to dq frame is a result of a combination of both Park and Clarke matrices.

3.1.2 Operating point evaluation in linearization

In this thesis work, the small signal modelling of a complex microgrid system by evaluating the complete state space model of microgrid system is initiated by determining the Operating point to linearize the non-linear model in its neighbourhood [78]. Given a non-linear set of state equations, the general form is given as;

$$\dot{x} = f(x,u)\,;\; y = g(x,u) \tag{3.5}$$

To find the linear equivalent of these non-linear equations, it is desired to evaluate an operating point about which the model can be safely considered as linear. These set of operating points (x_0 ,u_0) are calculated as;

$$0 = f(x_0, u_0)\ ;\ y_0 = g(x_0, u_0) \tag{3.6}$$

Thereafter, the model is linearized by finding the deviation about the operating point as;

$$\Delta x = x - x_0\ ;\ \Delta u = u - u_0\ ;\ \Delta y = y - y_0$$

There are several stable operating points about which a non-linear model can be linearized but once linearized the system stability can be analyzed only in the vicinity of that specific operating point around which it has been linearized.

3.1.3 State Perturbation

State perturbation is the analysis of perturb in the matrices constituting the state space representation of a system so as to study the impact of such a perturbation on the overall system dynamics. Such a perturb may occur due to variations in system parameters, component variations, uncertainties in loading, changes in operating conditions etc.

Given a state perturbation of ΔA in state space, as;

$$\dot{x} = (A + \Delta A)x \tag{3.7}$$

The perturbed eigen-triplets; i.e., eigenvalue $\Delta\lambda$, right eigenvectors $\Delta\emptyset_R$ and left eigenvectors $\Delta\emptyset_L$ of the perturbed system are given as;

$$(\emptyset_L + \Delta\emptyset_L)(A + \Delta A) = (\emptyset_L + \Delta\emptyset_L)(\lambda + \Delta\lambda) \tag{3.8}$$

$$(A + \Delta A)(\emptyset_R + \Delta\emptyset_R) = (\lambda + \Delta\lambda)(\emptyset_R + \Delta\emptyset_R) \tag{3.9}$$

The perturbations in state space modelling may even affect the small signal stability and hence, needs to be considered while evaluating the complete state space modelling of the complex system i.e., isolated microgrid system [16,79]. While a small state perturbation, ΔA may not alter a stable system, but the stability of a marginally stable system or systems on the boundary, such as those with very small real-valued poles, may shift towards the right half of s-plane and, hence system may become unstable. This is discussed in case 4 of Table 3.1 under 'Simulation Results'.

3.2 Small signal modelling of AC microgrid

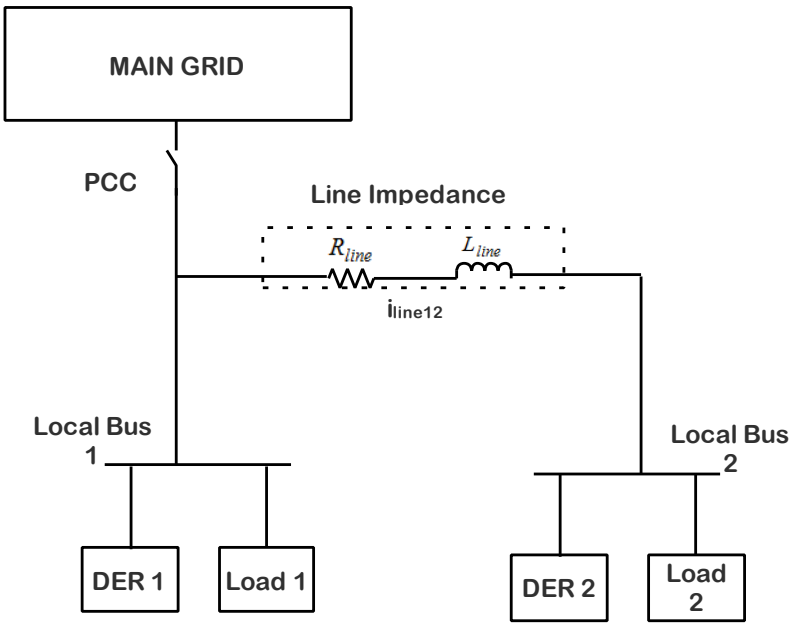

Figure 3.2. *AC Microgrid Architecture.*

In this work, a small signal model of an AC Microgrid system using conventional droop controlled invertor system has been developed. The individual DERs are connected to the load through a voltage source inverter circuit such that the gating pulses are

controlled through an inner and outer loop droop controller. The architecture of the microgrid is discussed in next section.

3.2.1 AC microgrid architecture

The microgrid architecture considered in this work is represented in Figure 3.2. It consists of two DERs connected to their individual local buses through LC filter and coupling inductances. The two local buses are coupled through a line of impedance $R_{line}+jXL_{line}$. When the Point of Common Coupling (PCC) is closed, the AC buses are connected to the main utility grid and hence, the microgrid works in 'Grid-tied mode'. Whereas, when PCC is open, then the microgrid is cut-off from the main grid and is in 'Autonomous mode'.

Although the small signal model of Microgrid exists in the literature as discussed in Chapter 2, the small signal model with necessary mathematical formulation has been obtained in this chapter for ease of the reader, as it is required in subsequent order reduction analysis in the preceding chapters. The small signal modelling of the system in Figure 3.3., requires the state space analysis of the two inverters, loads and line dynamics.

3.2.2 State space modelling in autonomous mode

Figure 3.3 shows the block diagram of an autonomous DG based inverter. The DG is connected to the load and common bus through a Voltage Source Inverter (VSI). The control strategy is this block diagram is implemented by three control loops: (a) outer power loop, which evaluates the desired frequency and voltage of the inverter through droop control technique; (b) Inner voltage control loop, which gives the reference currents through inductor; (c) Inner current control loop, which evaluates the reference voltages

to direct the State Vector Pulse Width Modulation (SVPWM) block to generate signal for the inverter [80].

The basic idea behind power sharing in the power controller block is to compensate any increase in the load side, in accordance with droop characteristics, through decrease in the frequency and voltage amplitude of the system [7]. The instantaneous active and reactive powers are calculated from the output currents and voltages. The average powers corresponding to the fundamental component are then obtained by passing these instantaneous powers through low pass filter with cut- off frequency of ω_c.

The reference frequency and voltage signals are therefore generated using conventional $P-\omega$ and $Q-V$ droop characteristic equations, such that,

$$\omega^r = \omega_n - mP \tag{3.10}$$

$$v_{oq}{}^r = V_{oq,n} - nQ \tag{3.11}$$

where, *m* and *n* are the static droop gain.

A *dq*-based Phase Locked Loop (PLL) with conventional PI strategy was chosen to measure the frequency of the system. The input signal to PLL block is the *d*-axis component of the voltage measured across the filter capacitor. In voltage control loop, the reference signals obtained from power controller are compared to the measured angular frequency from PLL block and measured q axis voltage by using conventional PI controllers. The reference inductor currents generated by voltage controller are compared by their measured values to obtain an error signal which thereby produces set-point voltage for input to SVPWM block. Reduced Total Harmonic Distortion (THD), simplified DSP implementation and fast processing makes, Space Vector Pulse Width Modulation advantageous over other PWM techniques. It lowers the frequency oscillation and is thus used in these microgrid systems.

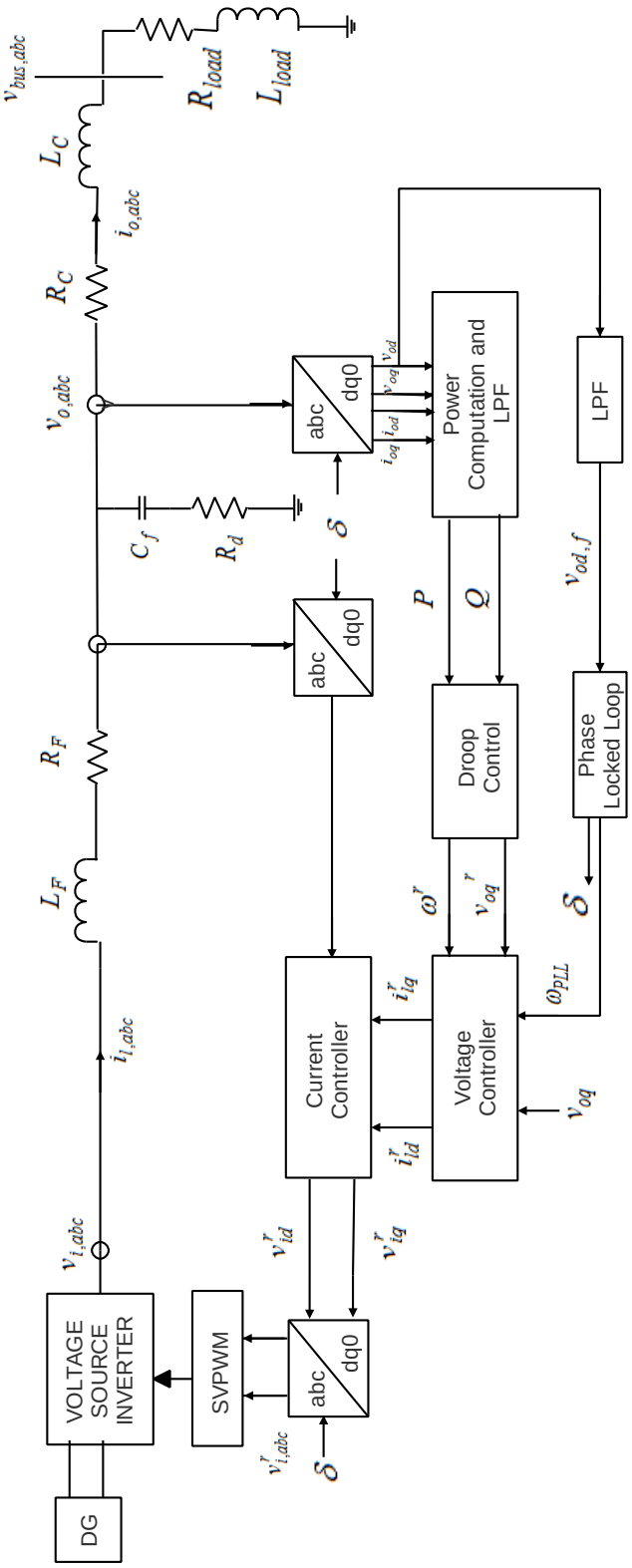

Figure 3.3. *Block diagram of Autonomous AC Microgrid.*

3.2.2.1 Local to global reference frame transformation

Generally in a microgrid system modelling, the load and line dynamics are referred in global reference frame, whereas each inverter is mathematically modelled in its own local frame (d-q). The individual inverter state equations are derived in terms of their individual local reference frame [10]. The input and output quantities of individual inverters can be transformed from their individual frame to a common reference frame (D-Q) using the transformation matrix as given (3.12).The angle θ, as shown in Figure 3.4., represents the angle between an individual inverter reference frame and the common global reference frame, which translates electrical quantities from local to common frame and vice versa.

$$T = \begin{bmatrix} \cos\theta & -\sin\theta \\ \sin\theta & \cos\theta \end{bmatrix} \tag{3.12}$$

where, $\theta = \int (\omega - \omega_{common})$

Considering the system to be autonomous, i.e., disconnected to main grid, the phase angle measured by the PLL of inverter 1 can be chosen as the reference for the overall interconnected system. The resultant reference angles calculated for both DERs can be used as;

$$\dot{\delta}_1 = \omega_{PLL1} - \omega_{PLL1} = 0 \tag{3.13}$$

$$\dot{\delta}_2 = \omega_{PLL1} - \omega_{PLL2} \tag{3.14}$$

where, ω_{PLL1} and ω_{PLL2} are calculated from DER1 and DER2, respectively.

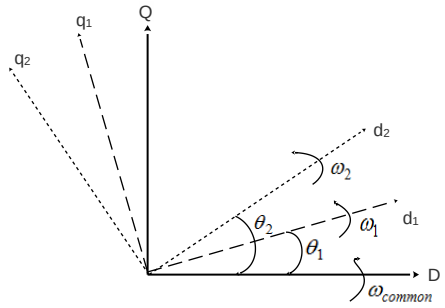

Figure 3.4. *Local to global reference frame transformation.*

3.2.2.2 Control scheme for VSI duty cycle regulation

The control scheme for the small signal model of the inverter is divided into several modules to enhance the understanding of the functionality of its various controllers involved.

Phase Locked Loop

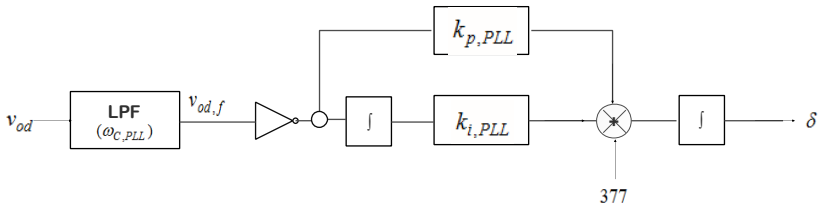

Figure 3.5. *Block diagram of PLL*

A *dq*-based PLL as in Figure 3.5. was chosen to measure the frequency of the system. The input signal to PLL is the *d*-axis component of the voltage measured across the filter capacitor. Therefore, the phase is locked such that $v_{od} = 0$. The PLL dynamics for measured frequency, ω_{PLL} and measured phase angle, δ are given as;

$$\dot{v}_{od,f} = \omega_{c.PLL}\, v_{od} - \omega_{c.PLL}\, v_{od,f}$$

$$\dot{\varphi_{PLL}} = -v_{od,f}$$

$$\omega_{PLL} = 377 - k_{p.PLL}\, v_{od,f} + k_{i.PLL}\, \varphi_{PLL}$$

$$\dot{\delta} = \omega_{PLL}$$

The resultant state equations from PLL as obtained by linearization around an equilibrium point are given below:

$$\Delta\dot{v}_{od,f} = \omega_{c.PLL}\, \Delta v_{od} - \omega_{c.PLL}\, \Delta v_{od,f} \tag{3.15}$$

$$\Delta\dot{\varphi}_{PLL} = -\Delta v_{od,f} \tag{3.16}$$

$$\Delta\dot{\delta} = -k_{p.PLL}\, \Delta v_{od,f} + k_{i.PLL}\, \Delta\varphi_{PLL} \tag{3.17}$$

Power Controller

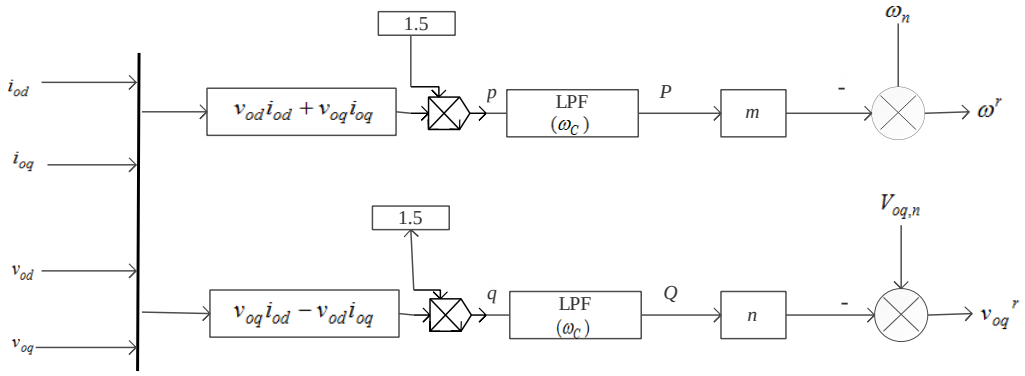

Figure 3.6. *Block diagram of Power Controller.*

The basic idea of power sharing function in the power controller module is to balance any increase in the load by decreasing the frequency and voltage amplitude of the system according to the droop characteristics. The instantaneous active and reactive powers are calculate from the output currents and voltages as shown in Figure 3.6 and given in (3.18-3.19). The average powers corresponding to the fundamental component are then obtained by passing these instantaneous powers through low pass filter with cut-off frequency of ω_c.

$$p = \frac{3}{2}\left(v_{od}i_{od} + v_{oq}i_{oq}\right) \tag{3.18}$$

$$q = \frac{3}{2}\left(v_{oq}i_{od} - v_{od}i_{oq}\right) \tag{3.19}$$

$$P = \frac{\omega_c}{s+\omega_c}\, p \Rightarrow \dot{P} = -P\omega_C + 1.5\omega_C\left(v_{od}i_{od} + v_{oq}i_{oq}\right)$$

$$Q = \frac{\omega_c}{s+\omega_c}\, q \Rightarrow \dot{Q} = -Q\omega_C + 1.5\omega_C\left(v_{od}i_{od} - v_{oq}i_{oq}\right)$$

The reference frequency and voltage signals are generated using conventional $P-\omega$ and $Q-V$ droop characteristic equations given in (3.10-3.11). The small signal dynamics of power controller is re-written after linearization as;

$$\Delta\dot{P} = -\omega_C\Delta P + 1.5\omega_C\left(V_{od}\Delta i_{od} + I_{od}\Delta v_{od} + V_{oq}\Delta i_{oq} + I_{oq}\Delta v_{oq}\right) \tag{3.20}$$

$$\Delta\dot{Q} = -\omega_C\Delta Q + 1.5\omega_C\left(V_{oq}\Delta i_{od} + I_{od}\Delta v_{oq} - V_{od}\Delta i_{oq} - I_{oq}\Delta v_{od}\right) \tag{3.21}$$

Voltage Controller

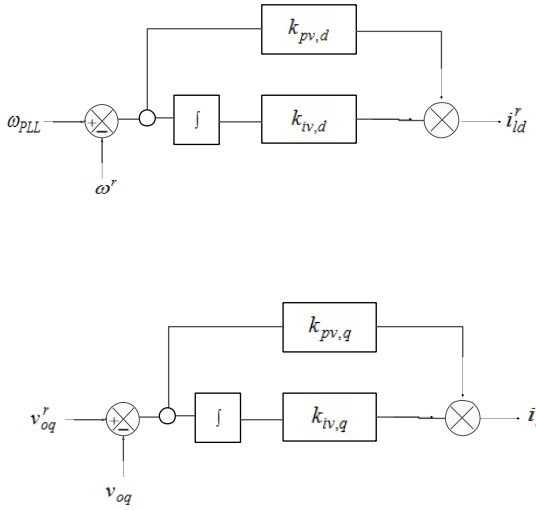

Figure 3.7. *Block diagram of Voltage Controller.*

In this block in Figure 3.7., the reference signals obtained from power controller are compared to the measured angular frequency from PLL block and measured q axis

voltage as shown in Figure 3.6. Conventional PI controllers are used in these controllers. As seen from the figure, the voltage controller equations are derived as;

$$\dot{\varphi_d} = \omega_{PLL} - \omega^r \;\; ; \qquad {i_{ld}}^r = k_{iv,d}\,\varphi_d + k_{pv,d}\,\dot{\varphi_d}$$

$$\dot{\varphi_q} = {v_{oq}}^r - v_{oq} \;\; ; \qquad {i_{lq}}^r = k_{iv,q}\,\varphi_q + k_{pv,q}\,\dot{\varphi_q}$$

The linearized state equations contributed by voltage controller to the inverter model are:

$$\Delta\dot{\varphi}_d = \Delta\omega_{PLL} + m\Delta P \tag{3.22}$$

$$\Delta\dot{\varphi}_q = -n\Delta Q - \Delta v_{oq} \tag{3.23}$$

Throughout the modelling process, all PI gains have been tuned by trial and error method.

Current Controller

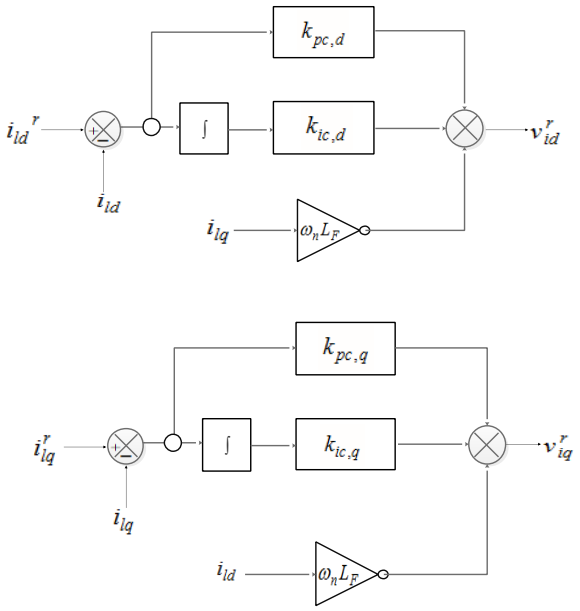

Figure 3.8. *Block diagram of current controller*.

The reference inductor currents generated by voltage controller are compared by their measured values to obtain an error signal which thereby produces set-point voltage for input to SVPWM block. The dynamical equations from current controller as in Figure 3.8. are:

$$\dot{\gamma}_d = {i_{ld}}^r - i_{ld} \; ; \quad {v_{id}}^r = -\omega_n L_f \, i_{lq} + k_{ic,d} \, \gamma_d + k_{pc,d} \dot{\gamma}_d$$

$$\dot{\gamma}_q = {i_{lq}}^r - i_{ld} \; ; \quad {v_{iq}}^r = \omega_n L_f \, i_{ld} + k_{ic,q} \, \gamma_q + k_{pc,q} \dot{\gamma}_q$$

The state equations contributed by current controller to the overall state space model dynamics are;

$$\Delta\dot{\gamma}_d = k_{iv,d} \, \Delta\varphi_d + k_{pv,d} \, \Delta\dot{\varphi}_d - \Delta i_{ld} \tag{3.24}$$

$$\Delta\dot{\gamma}_q = k_{iv,q} \, \Delta\varphi_q + k_{pv,q} \, \Delta\dot{\varphi}_q - \Delta i_{lq} \tag{3.25}$$

3.2.2.3 LC Filter and Coupling inductor model

A passive low-pass filter is used to attenuate switching frequency ripple. By considering the input and output voltages of inverter as equal, the state equations governing the filter dynamics derived by Kirchoff's laws are;

$$\dot{i}_{ld} = \frac{1}{L_f} \left(-r_f i_{ld} + v_{id} - v_{od}\right) + \omega_{PLL} i_{lq}$$

$$\dot{i}_{lq} = \frac{1}{L_f} \left(-r_f i_{lq} + v_{iq} - v_{oq}\right) + \omega_{PLL} i_{ld}$$

$$\dot{i}_{od} = \frac{1}{L_c} \left(-r_c i_{od} + v_{od} - v_{bd}\right) + \omega_{PLL} i_{oq}$$

$$\dot{i}_{oq} = \frac{1}{L_c} \left(-r_c i_{oq} + v_{oq} - v_{bq}\right) + \omega_{PLL} i_{od}$$

$$\dot{v}_{od} = \frac{1}{C_f} \left(i_{ld} - i_{od}\right) + \omega_{PLL} \, v_{oq} + R_d\left(\dot{i}_{ld} - \dot{i}_{od}\right)$$

$$\dot{v}_{oq} = \frac{1}{C_f} \left(i_{lq} - i_{oq}\right) - \omega_{PLL} \, v_{od} + R_d\left(\dot{i}_{lq} - \dot{i}_{oq}\right)$$

Thus, the six filter state space representation after small perturbation and subsequent linearisation of the above equations are given as;

$$\Delta\dot{i}_{ld} = -\frac{r_f}{L_F}\Delta i_{ld} + \frac{1}{L_F}\Delta v_{id} - \frac{1}{L_F}\Delta v_{od} + 377\Delta i_{lq} - k_{p.PLL} I_{lq}\,\Delta v_{od,f} - k_{p.PLL} V_{od,f}\Delta i_{lq} + k_{i.PLL}\, I_{lq}\Delta\varphi_{PLL} + k_{i.PLL}\emptyset_{PLL}\Delta i_{lq} \quad (3.26)$$

$$\Delta\dot{i}_{lq} = -\frac{r_f}{L_F}\Delta i_{lq} + \frac{1}{L_F}\Delta v_{iq} - \frac{1}{L_F}\Delta v_{oq} - 377\Delta i_{ld} + k_{p.PLL} I_{ld}\,\Delta v_{od,f} + k_{p.PLL} V_{od,f}\Delta i_{ld} - k_{i.PLL}\, I_{ld}\Delta\varphi_{PLL} - k_{i.PLL}\emptyset_{PLL}\Delta i_{ld} \quad (3.27)$$

$$\Delta\dot{i}_{od} = -\frac{r_c}{L_C}\Delta i_{od} + \frac{1}{L_C}\Delta v_{od} - \frac{1}{L_C}\Delta v_{bd} + 377\Delta i_{oq} - k_{p.PLL} I_{oq}\,\Delta v_{od,f} - k_{p.PLL} V_{od,f}\Delta i_{oq} + k_{i.PLL} I_{oq}\Delta\varphi_{PLL} + k_{i.PLL}\emptyset_{PLL}\Delta i_{oq} \quad (3.28)$$

$$\Delta\dot{i}_{oq} = -\frac{r_c}{L_C}\Delta i_{oq} + \frac{1}{L_C}\Delta v_{oq} - \frac{1}{L_C}\Delta v_{bq} - 377\Delta i_{od} + k_{p.PLL} I_{od}\,\Delta v_{od,f} + k_{p.PLL} V_{od,f}\Delta i_{od} - k_{i.PLL} I_{od}\Delta\varphi_{PLL} - k_{i.PLL}\emptyset_{PLL}\Delta i_{od} \quad (3.29)$$

$$\Delta\dot{v}_{od} = \frac{1}{C_F}(\Delta i_{ld} - \Delta i_{od}) + 377\Delta v_{oq} - k_{p.PLL} V_{oq}\,\Delta v_{od,f} - k_{p.PLL} V_{od,f}\Delta v_{oq} + k_{i.PLL} V_{oq}\Delta\varphi_{PLL} + k_{i.PLL}\emptyset_{PLL}\Delta v_{oq} + R_d\left(\Delta\dot{i}_{ld} - \Delta\dot{i}_{od}\right) \quad (3.30)$$

$$\Delta\dot{v}_{oq} = \frac{1}{C_F}\Delta i_{lq} - \frac{1}{C_F}\Delta i_{oq} - 377\Delta v_{od} + k_{p.PLL} V_{od}\,\Delta v_{od,f} + k_{p.PLL} V_{od,f}\Delta v_{od} - k_{i.PLL} V_{od}\Delta\varphi_{PLL} - k_{i.PLL}\emptyset_{PLL}\Delta v_{od} + R_d\left(\Delta\dot{i}_{lq} - \Delta\dot{i}_{oq}\right) \quad (3.31)$$

3.2.2.4 Load and line model

For the microgrid shown in Figure 3.3, the RL load dynamics for both the DERs, i.e., *i*=1,2, in the global D-Q frame are;

$$\dot{i}_{loadDi} = \frac{1}{L_{load}}(-R_{load} i_{loadDi} + v_{bDi}) + \omega_{PLLi} i_{loadQi}$$

$$\dot{i}_{loadQi} = \frac{1}{L_{load}}\left(-R_{load} i_{loadQi} + v_{bQi}\right) - \omega_{PLLi} i_{loadDi}$$

Considering the states Δx_{load} emerging from modelling of load of both the inverters, the load state space representation is given as;

$$\Delta x_{load} = [\Delta i_{loadD1} \quad \Delta i_{loadQ1} \quad \Delta i_{loadD2} \quad \Delta i_{loadQ2} \ ] \tag{3.32}$$

where,

$$\Delta \dot{\imath}_{loadD1} = -\frac{R_{load}}{L_{load_1}} \Delta i_{loadD1} + \frac{1}{L_{load_1}} \Delta v_{bD1} + 377\, \Delta i_{loadQ1} - k_{p,PLL}\, V_{od,f1}\, \Delta i_{loadQ1} - k_{p,PLL}\, I_{loadQ1}\, \Delta v_{od,f1} + k_{i,PLL}\, \emptyset_{PLL1}\, \Delta i_{loadQ1} + k_{i,PLL}\, I_{loadQ1}\, \Delta \emptyset_{PLL1} \tag{3.33}$$

$$\Delta \dot{\imath}_{loadQ1} = -\frac{R_{load}}{L_{load_1}} \Delta i_{loadQ1} + \frac{1}{L_{load_1}} \Delta v_{bQ1} - 377\, \Delta i_{loadD1} + k_{p,PLL}\, V_{od,f1}\, \Delta i_{loadD1} + k_{p,PLL}\, I_{loadD1}\, \Delta v_{od,f1} - k_{i,PLL}\, \emptyset_{PLL1}\, \Delta i_{loadD1} - k_{i,PLL}\, I_{loadD1}\, \Delta \emptyset_{PLL1} \tag{3.34}$$

$$\Delta \dot{\imath}_{loadD2} = -\frac{R_{load}}{L_{load_2}} \Delta i_{loadD2} + \frac{1}{L_{load_2}} \Delta v_{bD2} + 377\, \Delta i_{loadQ2} - k_{p,PLL}\, V_{od,f2}\, \Delta i_{loadQ2} - k_{p,PLL}\, I_{loadQ2}\, \Delta v_{od,f2} + k_{i,PLL}\, \emptyset_{PLL2}\, \Delta i_{loadQ2} + k_{i,PLL}\, I_{loadQ2}\, \Delta \emptyset_{PLL2} \tag{3.35}$$

$$\Delta \dot{\imath}_{loadQ2} = -\frac{R_{load}}{L_{load_2}} \Delta i_{loadQ2} + \frac{1}{L_{load_2}} \Delta v_{bQ2} - 377\, \Delta i_{loadD2} + k_{p,PLL}\, V_{od,f2}\, \Delta i_{loadD2} + k_{p,PLL}\, I_{loadD2}\, \Delta v_{od,f2} - k_{i,PLL}\, \emptyset_{PLL2}\, \Delta i_{loadD2} - k_{i,PLL}\, I_{loadD2}\, \Delta \emptyset_{PLL2} \tag{3.36}$$

In a similar way, the line model is considered to be in the form of a RL line impedance such that overall inductance represents the lumped line inductance and resistor represents the resistance due to losses in the long line. For the line impedance shown in figure 1, connected between bus 1 and bus 2, the line dynamics is given as;

$$\dot{\imath}_{lineDi\,j} = \frac{1}{L_{line}}\left(-r_{line} i_{lineD} + v_{bD,i} - v_{bD,j}\right) + \omega_{PLL} i_{lineQ}$$

$$\dot{\imath}_{lineDi\,j} = \frac{1}{L_{line}}\left(-r_{line} i_{lineQ} + v_{bQ,i} - v_{bQ,j}\right) + \omega_{PLL} i_{lineD}$$

The states contributed by line model are; $\Delta x_{line} = [\Delta i_{lineD21} \quad \Delta i_{lineQ21}]$; where,

$$\Delta \dot{\imath}_{lineD21} = -\frac{r_{line}}{L_{line}} \Delta i_{lineD21} + \frac{1}{L_{line}} \Delta v_{bD2} - \frac{1}{L_{line}} \Delta v_{bD1} + 377\, \Delta i_{lineQ21} - k_{p,PLL}\, V_{od,f1}\, \Delta i_{lineQ21} - k_{p,PLL}\, I_{lineQ21}\, \Delta v_{od,f1} + k_{i,PLL}\, \emptyset_{PLL1}\, \Delta i_{lineQ21} + k_{i,PLL}\, I_{lineQ21}\, \Delta \emptyset_{PLL1} \tag{3.37}$$

$$\Delta \dot{\imath}_{lineQ21} = -\frac{r_{line}}{L_{line}}\,\Delta i_{lineQ21} + \frac{1}{L_{line}}\,\Delta v_{bQ2} - \frac{1}{L_{line}}\,\Delta v_{bQ1} - 377\,\Delta i_{lineD21} + k_{p,PLL}\,V_{od,f1}\,\Delta i_{lineD21} + k_{p,PLL}\,I_{lineD21}\,\Delta v_{od,f1} - k_{i,PLL}\,\emptyset_{PLL1}\,\Delta i_{lineD21} - k_{i,PLL}\,I_{lineD21}\,\Delta \emptyset_{PLL1} \quad (3.38)$$

3.2.2.5 State Space Representation of autonomous AC microgrid system

The solution of nonlinear state equations, results in numerous operating points as discussed in Section 3.1. All these operating points, when substituted in the system model converge in a unique set of eigenvalues and hence, stability remains constant irrespective of the operating point used. Two operating points are used for linearization in this thesis work, as in the order in equation (3.45), which are given below;

X_{oper1}=[0 427.5168617327 70.6170034059 0.0023046622 0.1341087489 0.0006727867 0.8659982689 0.0755690319 3.356108065 0.0238838476 84.9226043131 0.5553074851 3.3559731423 -0.1928204754 0.0238838472 -0.0028025069 319.8844680459 99.8188550535 0.0128811824 0.1005479992 0.0015581691 0.8615899257 0.3040973201 2.511731333 0.0000000083 84.9041184384 0.7837770177 2.5117313328 -0.1778744746 0.0000000083 0.7498537394 3.2112097558 0.4024841940 3.3356768754 0.1545880693 -0.0685844362]^T

X_{oper2}=[0 391.3662706302 72.05087785541 0.003603224363 0.122404418455 0.000436238942 0.864378130696 0.085978348802 3.073085590603 -0.004599444120 84.90204136555 0.565590507310 3.07311157262 -0.20035814421 -0.004599444084 0.000800633243 407.4322324061 27.91019451458 -0.01052206978 0.126689262146 -0.001228432831 0.865079063267 -0.260438434021 3.198991901613 0.001816807069 84.908612346102 0.2192074870664 3.1989816386079 -0.200875022866

0.001816807054 0.746751476846 3.212185062451 0.397813605348 3.338168700060 0.1816841344989 0.2235924503283]^{T} (3.39)

The complete small signal modelling of the two inverter architecture as in Figure 3.2 is achieved by combining the models of the two inverters into a one state space as given[10];

$$\boldsymbol{x_{inv1}} = [\delta_1\ P_1\ Q_1 \varphi_{d1} \varphi_{q1} \gamma_{d1} \gamma_{q1} i_{ld1} i_{lq1} v_{od1} v_{oq1} i_{od1} i_{oq1} \varphi_{PLL1} v_{od1,f}] \tag{3.40}$$

$$\boldsymbol{x_{inv2}} = [\delta_2\ P_2\ Q_2 \varphi_{d2} \varphi_{q2} \gamma_{d2} \gamma_{q2} i_{ld2} i_{lq2} v_{od2} v_{oq2} i_{od2} i_{oq2} \varphi_{PLL2} v_{od2,f}] \tag{3.41}$$

$$\boldsymbol{x_{inv}} = [\boldsymbol{x_{inv1}} \boldsymbol{x_{inv2}}] \tag{3.42}$$

The collective load and line model from the two inverters is given as, $\boldsymbol{x_{load}} = [i_{loadD1}\ i_{loadQ1}\ i_{loadD2}\ i_{loadQ2}]$ and$\boldsymbol{x_{line}} = [i_{lineD21}\ i_{lineQ21}]$.

After linearization of the complete system about stable operating points as given and rearranging the state variables and output variables in order as in (3.45-3.46), the complete 36th order state space model for the autonomous microgrid system is obtained from as;

$$\Delta \dot{\boldsymbol{x}} = \boldsymbol{A}\Delta \boldsymbol{x} + \boldsymbol{B}\Delta \boldsymbol{u} \tag{3.43}$$

$$\Delta \boldsymbol{y} = \boldsymbol{C}\Delta \boldsymbol{x} \tag{3.44}$$

where; $\boldsymbol{A}$ is the state matrix (36×36)**,** $\boldsymbol{B}$ is the input matrix (36×4) and $\boldsymbol{C}$ is the output matrix (6×36)

State vector, $\boldsymbol{x} = [\boldsymbol{x_{inv1}} \quad \boldsymbol{x_{inv2}} \quad \boldsymbol{x_{load}} \quad \boldsymbol{x_{line}}]^T$ (3.45)

Output vector, $\boldsymbol{y} = \left[\Delta i_{oDQ1}\ \ \Delta i_{oDQ2}\ \ \Delta \omega_{PLL1}\ \ \Delta \omega_{PLL2}\right]^T$ (3.46)

Input vector, $\boldsymbol{u} = \left[\Delta v_{bD1}\ \ \Delta v_{bQ1}\ \ \Delta v_{bD2}\ \ \Delta v_{bQ2}\right]^T$ (3.47)

Thus, the small signal model of autonomous AC microgrid with state space representations as in (3.43-3.44) will be deployed for further analysis on its reduced order modelling in the next chapter.

3.2.3 State space modelling in grid-tied mode

The simplified architecture of the 3-phase inverter based Grid-tied microgrid system is given in Figure 3.9. With the Point of Common Coupling (PCC) closed, the microgrid operates in a grid-connected mode such that the link between main utility grid and DER exists.

When the microgrid is connected to the main utility grid, the bus voltage and system frequency are controlled by the main grid. The objective of this mode is to regulate the active and reactive powers to follow their commanded values, P^r andQ^r, given as system inputs. The schematic of the grid-tied system in Figure 3.10, consists of Phase Locked Loop (PLL) block, power computation block, power controller and current controller blocks connected to the three phase Voltage-Source Inverter (VSI).

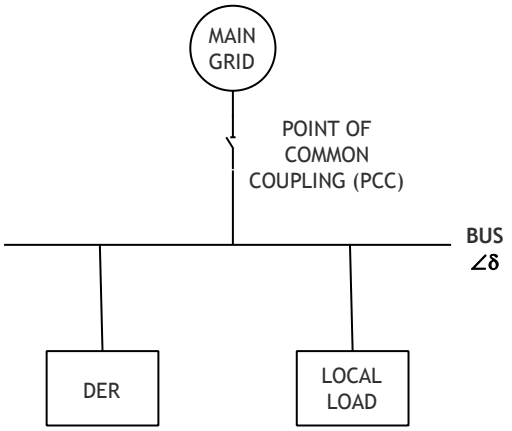

Figure 3.9. *Grid-tied Microgrid Architecture.*

The grid-tied microgrid structure consists of two control loops: an outer power control loop and an inner current control loop. The PLL block measures the system phase angle which in turn synchronizes all the abc to dq and dq to abc converters in the system. The measured output currents and voltages in both d-q axes serve as inputs for power calculation in the outer loop. The computed active and reactive powers, P and$Q$, are subsequently compared with the reference powers in the power controller block. Thereafter, the reference inductor currents generated by the power controller are compared to their measured values in the current controller, to obtain an error signal which is given to the State Vector Pulse Width Modulation (SVPWM) block, thereby generating switching pulses. The voltages at the input and output of the VSI are assumed to be the same, i.e. $v_{i,abc} = {v_{i,abc}}^{r}$. The utility of SVPWM in this system results from its quality of lowering the fluctuations on the system frequency.

3.2.3.1 Local to global reference frame transformation

The small signal modelling of the grid-tied microgrid system requires a frame transformation of individual DER to the global reference frame as also discussed for autonomous microgrid in Section 3.1.1. The small signal model of a microgrid system calculated in the local reference frame (d-q) is translated to the global reference frame of the main grid by using the orthogonal transformation matrix as in [13], which is reproduced in equation (3.48).

$$\boldsymbol{A}_{DQ}^{global} = \begin{bmatrix} \cos\theta & -\sin\theta \\ \sin\theta & \cos\theta \end{bmatrix} \boldsymbol{A}_{dq}^{local} \tag{3.48}$$

where, $\theta = \delta = \int(\omega - \omega_{common})$ as in Figure 3.11.

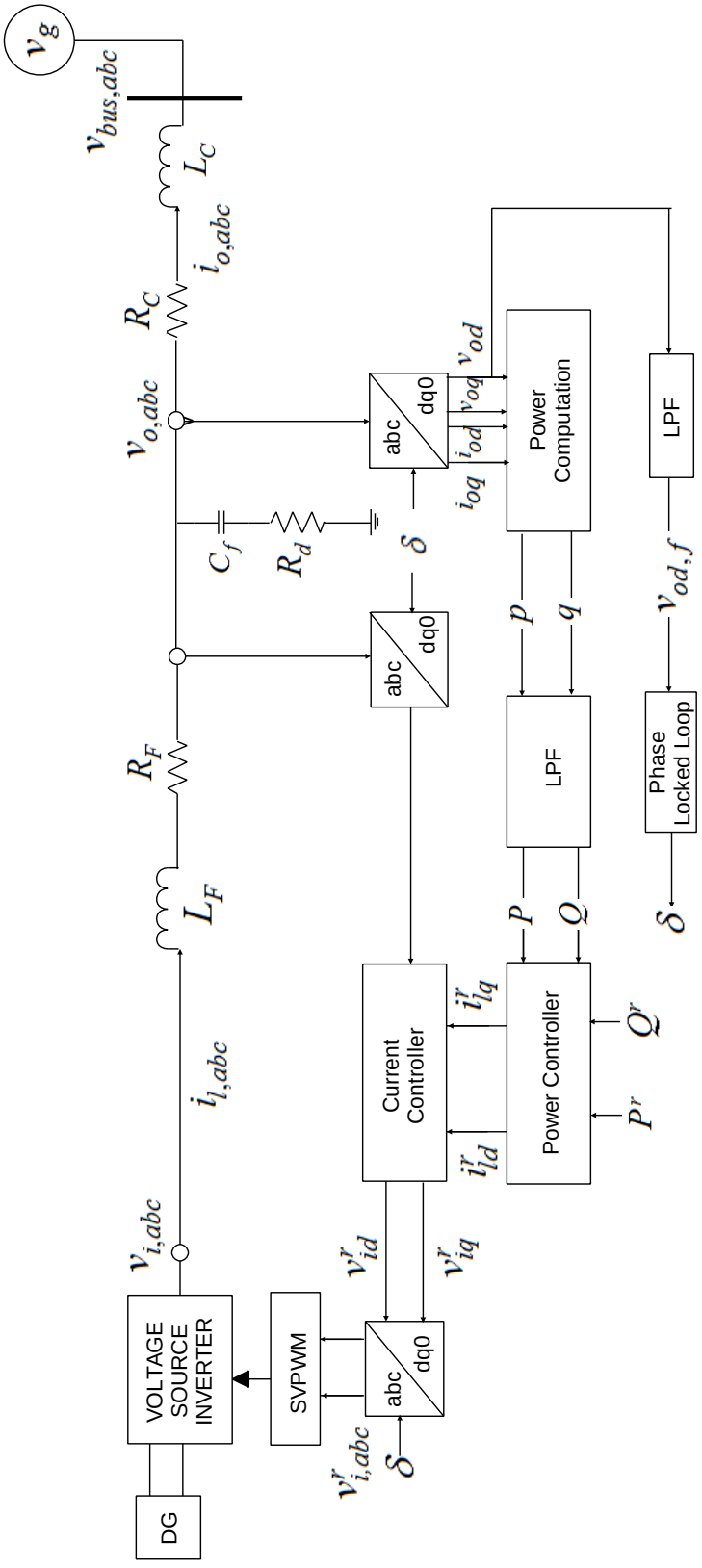

Figure 3.10. *Schematic of the Grid-tied Microgrid System.*

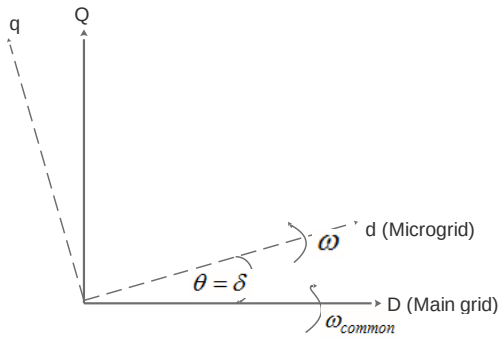

Figure 3.11. *Reference frame transformations.*

3.2.3.2 Control scheme for VSI duty cycle regulation

The several blocks discussed for control scheme of microgrid system in this section are: PLL block, Power computation block, Power controller, Current controller, LC Filter and coupling inductor.

Phase Locked Loop

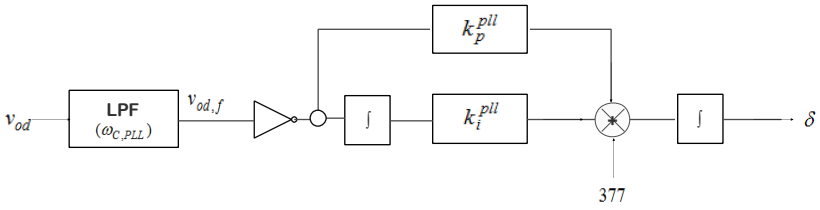

Figure 3.12. *Block diagram of PLL.*

A *dq*-based PLL was chosen to measure the frequency of the system. The input signal to PLL is the *d*-axis component of the voltage measured across the filter capacitor. Therefore, the phase is locked such that $v_{od} = 0$. The PLL dynamics for measured frequency, ω_{PLL} and measured phase angle, δ are given as;

$$\dot{v}_{od,f} = \omega_{c.PLL}\, v_{od} - \omega_{c.PLL}\, v_{od,f}$$

$$\dot{\varphi_{PLL}} = -v_{od,f}$$

$$\omega_{PLL} = 377 - k_{p.PLL}\, v_{od,f} + k_{i.PLL}\, \varphi_{PLL}$$

$$\dot{\delta} = \omega_{PLL}$$

The linearized state equations from PLL are;

$$\Delta\dot{v}_{od,f} = \omega_{c.PLL}\, \Delta v_{od} - \omega_{c.PLL}\, \Delta v_{od,f} \tag{3.49}$$

$$\Delta\dot{\varphi_{PLL}} = -\Delta v_{od,f} \tag{3.50}$$

$$\Delta\dot{\delta} = -k_{p.PLL}\, \Delta v_{od,f} + k_{i.PLL}\, \Delta\varphi_{PLL} \tag{3.51}$$

Power Calculation

The instantaneous active and reactive powers are calculated from the output currents and voltages as shown in Figure 3.13 and given in (3.52-3.53).

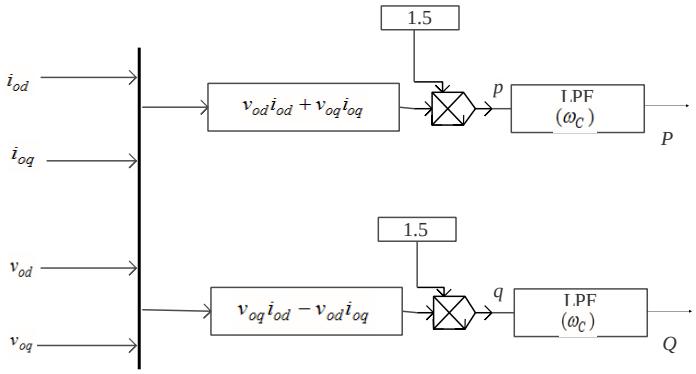

Figure 3.13. *Diagram of Power Computation block.*

$$p = \frac{3}{2}\left(v_{od}i_{od} + v_{oq}i_{oq}\right) \tag{3.52}$$

$$q = \frac{3}{2}\left(v_{oq}i_{od} - v_{od}i_{oq}\right) \tag{3.53}$$

The average powers corresponding to the fundamental component are then obtained by passing these instantaneous powers through low pass filter with cut-off frequency of ω_c.

$$P = \frac{\omega_c}{s + \omega_c}\, p \Rightarrow \dot{P} = -P\omega_C + 1.5\omega_C\left(v_{od}i_{od} + v_{oq}i_{oq}\right)$$

$$Q = \frac{\omega_c}{s + \omega_c}\, q \Rightarrow \dot{Q} = -Q\omega_C + 1.5\omega_C\left(v_{od}i_{od} - v_{oq}i_{oq}\right)$$

The small signal dynamics of power controller is re-written after linearization as;

$$\Delta\dot{P} = -\omega_C\Delta P + 1.5\omega_C\left(V_{od}\Delta i_{od} + I_{od}\Delta v_{od} + V_{oq}\Delta i_{oq} + I_{oq}\Delta v_{oq}\right) \tag{3.54}$$

$$\Delta\dot{Q} = -\omega_C\Delta Q + 1.5\omega_C\left(V_{oq}\Delta i_{od} + I_{od}\Delta v_{oq} - V_{od}\Delta i_{oq} - I_{oq}\Delta v_{od}\right) \tag{3.55}$$

Power Controller

In this block, the active and reactive power set point signals are compared to their corresponding measured signals from power computation block as shown in Figure 3.14.

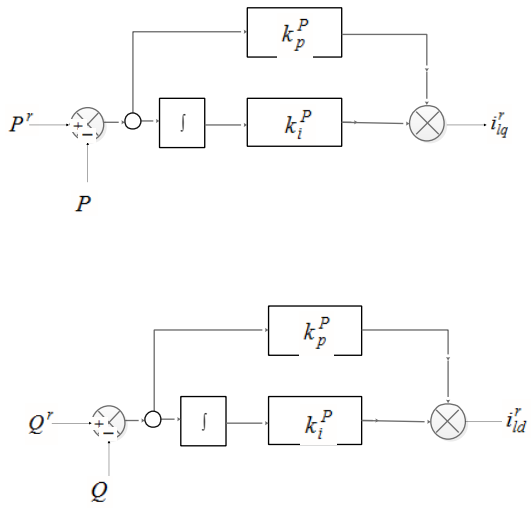

Figure 3.14. *Block diagram of Power Controller.*

Conventional PI controllers are used in these controllers. As seen from the figure, the power controller equations are derived as;

$$\dot{\varphi_P} = P^r - P \; ; \; {i_{lq}}^r = {k_i}^P \varphi_P + {k_p}^P \dot{\varphi_P}$$

$$\dot{\varphi_Q} = Q^r - Q \; ; \; {i_{ld}}^r = {k_i}^P \varphi_Q + {k_p}^P \dot{\varphi_Q}$$

The state equations contributed by voltage controller to the inverter model are:

$$\Delta\dot{\varphi}_P = \Delta P^r - \Delta P \tag{3.56}$$

$$\Delta\dot{\varphi}_Q = \Delta Q^r - \Delta Q \tag{3.57}$$

Current Controller

The reference inductor currents generated by the voltage controller are compared by their measured values to obtain a resultant error signal. This signal thereby produces a set-point voltage for input to SVPWM block, subsequently generating switching pulses.

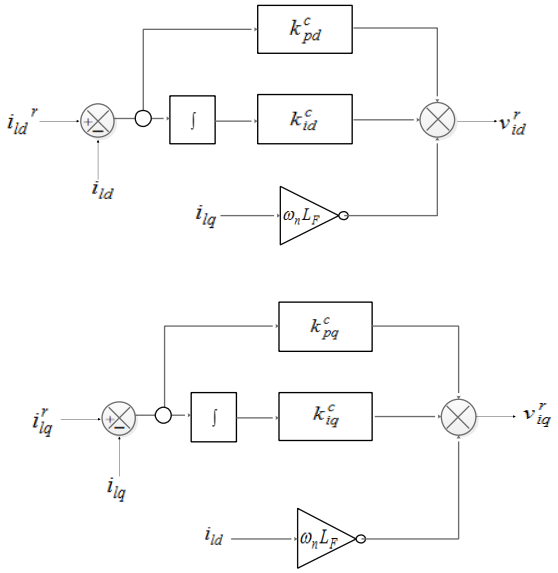

***Figure 3.15**. Block diagram of current controller.*

The dynamical equations from current controller as in Figure 3.15. are;

$$\dot{\gamma}_d = {i_{ld}}^r - \ i_{ld} \ ; \ {v_{id}}^r = \ - \omega_n L_f \ i_{lq} + \ {k_i}^C \ \gamma_d + \ {k_p}^C \dot{\gamma}_d$$

$$\dot{\gamma}_q = {i_{lq}}^r - \ i_{ld} \ ; \ {v_{iq}}^r = \ \omega_n L_f \ i_{ld} + \ {k_i}^C \ \gamma_q + \ {k_p}^C \dot{\gamma}_q$$

The state equations contributed by current controller to the overall state space model dynamics are;

$$\Delta\dot{\gamma}_d = {k_i}^P \ \Delta\varphi_d + {k_p}^P \ \Delta\dot{\varphi}_d - \ \Delta i_{ld} \tag{3.58}$$

$$\Delta\dot{\gamma}_q = {k_i}^P \ \Delta\varphi_q + {k_p}^P \ \Delta\dot{\varphi}_q - \ \Delta i_{lq} \tag{3.59}$$

3.2.3.3 LC Filter and Coupling inductor

A passive low-pass filter is used to attenuate switching frequency ripple. By considering the input and output voltages of inverter as equal, the state equations governing the filter dynamics can be given as;

$$\dot{i}_{ld} = \frac{1}{L_f} \left(-r_f i_{ld} + \ v_{id} - v_{od}\right) + \ \omega_n i_{lq}$$

$$\dot{i}_{lq} = \frac{1}{L_f} \left(-r_f i_{lq} + \ v_{iq} - v_{oq}\right) + \ \omega_n i_{ld}$$

$$\dot{i}_{od} = \frac{1}{L_c} \left(-r_c i_{od} + \ v_{od} - v_{bd}\right) + \ \omega_n i_{oq}$$

$$\dot{i}_{oq} = \frac{1}{L_c} \left(-r_c i_{oq} + \ v_{oq} - v_{bq}\right) + \ \omega_n i_{od}$$

$$\dot{v}_{od} = \frac{1}{C_f} \left(i_{ld} - i_{od}\right) + \ \omega_n \ v_{oq} + R_d\left(\dot{i}_{ld} - \dot{i}_{od}\right)$$

$$\dot{v}_{oq} = \frac{1}{C_f} \left(i_{lq} - i_{oq}\right) - \ \omega_n \ v_{od} + R_d\left(\dot{i}_{lq} - \dot{i}_{oq}\right)$$

Thus, the six equations in filter state space repreentation after small perturbation and subsequent linearisation are given as;

$$\Delta\dot{i}_{ld} = -\left(\frac{r_f}{L_F}+\frac{k_p^C}{L_F}\right)\Delta i_{ld}+\frac{k_i^C}{L_F}\Delta\gamma_d+\frac{k_p^C k_i^P}{L_F}\Delta\emptyset_Q+\frac{k_p^C k_p^P}{L_F}\Delta Q^r-\frac{k_p^C k_p^P}{L_F}\Delta Q-\frac{1}{L_F}\Delta v_{od} \quad (3.60)$$

$$\Delta\dot{i}_{lq} = -\left(\frac{r_f}{L_F}+\frac{k_p^C}{L_F}\right)\Delta i_{lq}+\frac{k_i^C}{L_F}\Delta\gamma_q+\frac{k_p^C k_i^P}{L_F}\Delta\emptyset_Q+\frac{k_p^C k_p^P}{L_F}\Delta P^r-\frac{k_p^C k_p^P}{L_F}\Delta P-\frac{1}{L_F}\Delta v_{oq} \quad (3.61)$$

$$\Delta\dot{i}_{od} = -\left(\frac{2R_C}{L_C}-\frac{R_F}{L_F}-R_d\right)\Delta i_{od}+\frac{1}{L_C}\Delta v_{od}-\frac{1}{L_C}\Delta v_{oq}+R_d\Delta i_{ld}+\omega_n\Delta i_{oq} \quad (3.62)$$

$$\Delta\dot{i}_{oq} = -\left(\frac{2R_C}{L_C}-\frac{R_F}{L_F}-R_d\right)\Delta i_{oq}+\frac{1}{L_C}\Delta v_{oq}-\frac{1}{L_C}(-k_p^{pll}\Delta v_{od,f}+k_i^{pll}\Delta\emptyset_{PLL})-R_d\Delta i_{lq}-$$
$$\omega_n\Delta i_{od} \quad (3.63)$$

$$\Delta\dot{v}_{od} = \left(\frac{1}{C_F}-\frac{R_d\left(R_F+k_p^C\right)}{L_F}-{R_d}^2\right)\Delta i_{ld}-\left(\frac{1}{C_F}-\frac{R_d(R_C-R_F)}{L_F}-\frac{R_d R_C}{L_C}+{R_d}^2\right)\Delta i_{od}$$
$$+\left(\omega_n+\frac{R_d}{L_C}\right)\Delta v_{oq}+\frac{k_i^C R_d}{L_F}\Delta\gamma_d+\frac{k_p^C k_i^P R_d}{L_F}\Delta\emptyset_Q+\frac{k_p^C k_p^P R_d}{L_F}\Delta Q^r-\frac{k_p^C k_p^P R_d}{L_F}\Delta Q-$$
$$R_d\left(\frac{1}{L_F}+\frac{1}{L_C}\right)\Delta v_{od}-R_d\omega_n\Delta i_{oq} \quad (3.64)$$

$$\Delta\dot{v}_{oq} = \left(\frac{1}{C_F}-\frac{R_d\left(R_F+k_p^C\right)}{L_F}-{R_d}^2\right)\Delta i_{lq}-\left(\frac{1}{C_F}-\frac{R_d(R_C-R_F)}{L_F}-\frac{R_d R_C}{L_C}+{R_d}^2\right)\Delta i_{oq}$$
$$+\omega_n\Delta v_{od}+\frac{k_i^C R_d}{L_F}\Delta\gamma_q+\frac{k_p^C k_i^P R_d}{L_F}\Delta\emptyset_P+\frac{k_p^C k_p^P R_d}{L_F}\Delta P^r-\frac{k_p^C k_p^P R_d}{L_F}\Delta P-R_d\left(\frac{1}{L_F}+\right.$$
$$\left.\frac{1}{L_C}\right)\Delta v_{oq}-R_d\omega_n\Delta i_{od}+\frac{R_d}{L_C}\left(-k_p^{pll}\Delta v_{od,f}+k_i^{pll}\Delta\emptyset_{PLL}\right) \quad (3.65)$$

3.2.3.4 State space representation of grid-tied AC microgrid system

The non-linear dynamic model of the microgrid system is linearized at an equilibrium point which is evaluated as in Section 3.2.2.

$$X_{oper}=[0.0000036106\ -0.0000019850\ \ -0.000000007\ -188.5000000045\ 0\ 0.0189001525\ -0.0106497444\ \ -0.0000053247\ \ 0.0000220378\ \ -0.0010649465\ \ 0.0018899647\ -0.0010578279\ 0.0019241120\ -0.0000000072\ 0.0012588128]^T \quad (3.66)$$

The modelled linear-system is an approximation of the non-linear system model and is valid only for the equilibrium point about which the non-linear system is linearized. It is known from Lyapunov's first method that if the linear system is stable then the non-linear system is also stable at the equilibrium point. The complete state space representation of a grid-connected microgrid system is;

$$\Delta \dot{\boldsymbol{x}} = \boldsymbol{A}\Delta \boldsymbol{x} + \boldsymbol{B}\Delta \boldsymbol{u},\ \Delta \boldsymbol{y} = \boldsymbol{C}\Delta \boldsymbol{x} \tag{3.67}$$

where,

$$\Delta x = [\,\Delta P\ \ \Delta Q\ \ \Delta v_{od,f}\ \ \Delta\varphi_{PLL}\ \Delta\delta\ \ \Delta\varphi_P\,\Delta\varphi_Q\ \ \Delta\gamma_d\ \Delta\gamma_q\ \Delta i_{ld}\ \ \Delta i_{lq}\ \ \Delta i_{od}\ \ \Delta i_{oq}\ \Delta v_{od}\,\Delta v_{oq}]^T \tag{3.68}$$

$$\Delta y = \left[\Delta P\quad \Delta Q\quad \Delta i_{od}\ \ \Delta i_{oq}\quad \Delta i_{ld}\ \ \Delta i_{lq}\quad \Delta v_{od}\ \ \Delta v_{oq}\ \ \Delta\omega_{PLL}\right]^T \tag{3.69}$$

$\Delta u = [P^r\ Q^r]^{\,T}$ are state variables, output variables and input variables respectively.

Thus, the small signal model of grid-tied AC microgrid with state space representations as in (3.67) will be deployed for further analysis based on its reduced order modelling in chapter 4.

3.3 Small Signal Modelling of DC Microgrid

The PV-fuel cell based DC microgrid considered in this work has been shown in Figure 3.16 and its small signal model is given as below.

3.3.1 DC microgrid architecture

The autonomous DC microgrid block diagram in Figure 3.16, shows the interconnected system components comprising of two sources: PV array and fuel cell stack along with individual storage devices to supply uninterrupted power to the DC load.

The converter interfaced sources are directly connected to DC bus which subsequently supplies the load requirements. The aggregation of different feasible load combinations are depicted by an equivalent load model comprising of Constant Resistive Load (CRL) and Constant Voltage Load (CVL) [26] in present analysis.

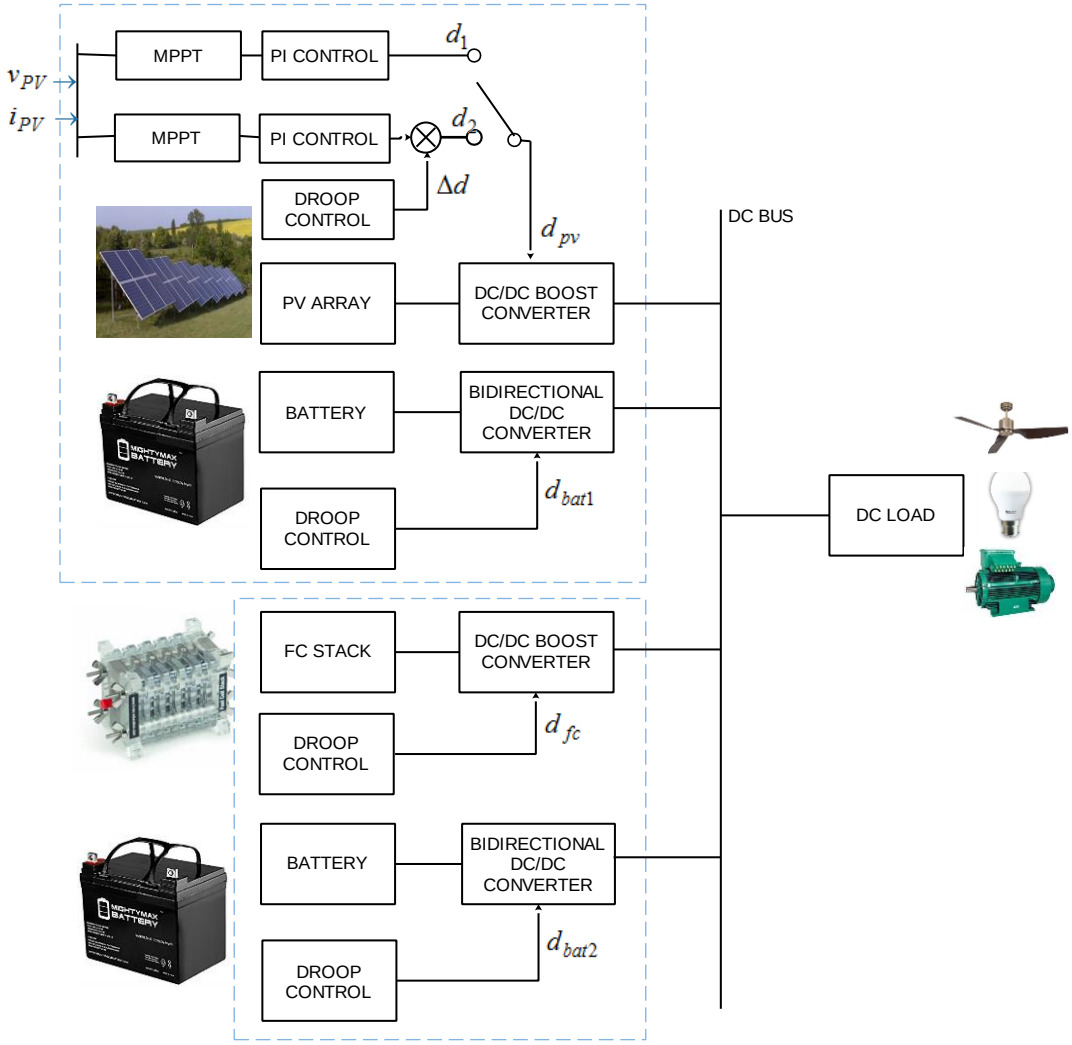

Figure 3.16. *Block diagram of PV-fuel cell based DC microgrid system.*

The control strategies involved in this work are limited to MPPT and droop control for accurate fulfilment of load power through regulation of converter duty cycle ratio. A decentralised modified droop control ensuring both accuracy in current sharing and

voltage restoration for each converter model has been utilised for effective load power sharing [27]. MPPT controller tracks the maximum power points of a PV array by adjusting the converter duty cycle. A droop control in combination with MPPT controller has been explored to meet the load requirements in the system.

3.3.2 Microgrid component modelling

In this section, a mathematical model is presented for all the subsystems in DC microgrid architecture as in Figure 3.16. The main subsystems are PV, fuel cell, DC/DC boost converter, storage system, load and line. The complete microgrid model is developed after individual subsystem modelling.

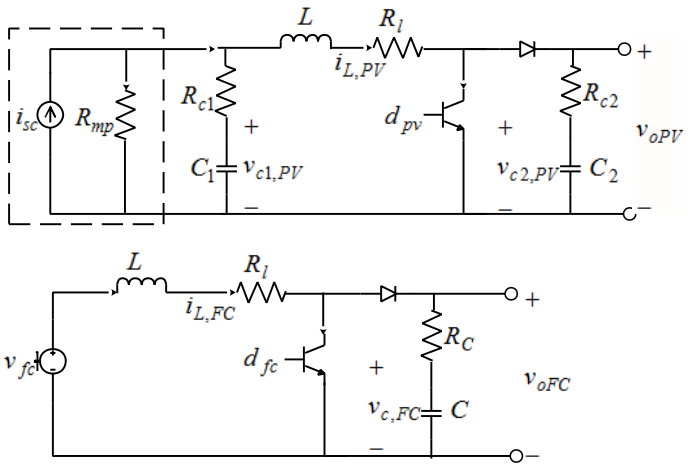

Figure 3.17. *PV and fuel cell with DC/DC boost converter.*

3.3.2.1 Photovoltaic array with DC/DC boost converter

A simplified Norton equivalent PV module involving short-circuit current i_{sc} and PV voltage and current at maximum power point, i.e., V_{MPP} and I_{MPP} respectively as shown in Figure 3.17., is connected to a DC boost converter electrical model. Norton

equivalent model is used to demonstrate the effect of irradiance uncertainties on the overall system functionality [22].

Considering parasitic losses associated with converter elements in the form of resistancesR_{c1}, R_{c2}, R_l, the states associated with inductor current $i_{L,PV}$ and capacitor voltages $v_{c1,PV}$ and $v_{c2,PV}$ are expressed in the following equation.

$$i_{L,PV} = \frac{R_{mp}R_{c1}}{R_{mp}+R_{c1}}\frac{i_{sc}}{L} + \frac{R_{mp}}{R_{mp}+R_{c1}}\frac{v_{c1}}{L} - \left(\frac{R_{mp}R_{c1}}{R_{mp}+R_{c1}} + R_L\right)\frac{1}{L}i_{L,PV} - \frac{1}{L}\,v_{oPV}\,(1-d_{pv})$$

$$\dot{v}_{c1,PV} = \frac{R_{mp}}{C_1(R_{mp}+R_{c1})}i_{sc} - \frac{R_{mp}}{C_1(R_{mp}+R_{c1})}i_{L,PV} - \frac{1}{C_1(R_{mp}+R_{c1})}v_{c1,PV},$$

$$\dot{v}_{c2,PV} = \frac{1}{R_{c2}C_2}\,v_{oPV} - \frac{1}{R_{c2}C_2}\,v_{c2,PV} \tag{3.70}$$

where, d_{pv} is the converter duty ratio determined by droop and MPPT controller as in (3.91).

3.3.2.2 Fuel cell stack with DC/DC boost converter

An approximate model of fuel cell consists of a single electrical state variable representing voltage across a capacitor formed from the charge decomposition on the electrodes [24]. This is also known as 'double-charge effect'. Contrary to the usual fuel cell electrical model, reference [23, 81] gives a detailed state space analysis of the various electrical and non-electrical fuel cell states taking the effect of chemical and electrochemical processes into account. An accurate state space representation of DC microgrid system takes into consideration the effect of these processes into the overall system dynamical behaviour. In this context, the state space model in [23] (consisting of 11 state variables) will be incorporated into the DC microgrid state space model to demonstrate their effects in terms of nonlinearity and sluggish time responses. These states are defined as follows.

$$\boldsymbol{x_{fc}} = [(m_{O_2})_{net};\ (m_{H_2})_{net};\ (m_{H_2O})_{net};\ T; P_{H_2}; P_{O_2}; P_{H_2O}; Q_C;\ Q_E;\ Q_L;\ v_{cd}] \quad (3.71)$$

where, $(m_{O_2})_{net}$, $(m_{H_2})_{net}$ and , $(m_{H_2O})_{net}$ are net mole flow rate of oxygen, hydrogen and water respectively; T indicates the stack temperature; P_{H_2}, P_{O_2} and P_{H_2O} are the partial pressures of hydrogen, oxygen and water respectively; Q_C is the heat generated due to electrochemical reaction, Q_E is the heat generated due to electricity and Q_L is the heat loss by air convection; v_{cd} represents the voltage across capacitance due to 'double-layer charge effect'.

Following the similar approach as for PV-converter modelling, the boost converter state equations are given as,

$$i_{L,FC} = \frac{1}{L}\, v_{fc} - \frac{R_L}{L}\, i_L - \frac{1}{L}\, v_{oFC}\,(1 - d_{fc}),$$

$$\dot{v}_{c,FC} = \frac{1}{CR_c} v_{oFC} - \frac{1}{CR_c} v_{c,FC} \quad (3.72)$$

where, d_{fc} is the duty ratio of converter interfacing fuel cell determined by droop controller in (3.86).

3.3.2.3 Battery with bidirectional converter

A mathematical model of storage batteries connected to bidirectional DC/DC converter for each of the sources, as in Figure 3.18., is derived by writing Kirchhoff's current and voltage laws and given in [25].

$$i_{bat1} = -\frac{R_{s1}}{L_{bat1}} i_{bat1} - \frac{1}{L_{bat1}} v_{c1,B} - \frac{1}{L_{bat1}} d_{bat1} v_{oPV} + \frac{1}{L_{bat1}} e_{01},\ i_{bat2} = -\frac{R_{s2}}{L_{bat2}} i_{bat2} - \frac{1}{L_{bat2}} v_{c2,B} - \frac{1}{L_{bat2}} d_{bat2} v_{oFC} + \frac{1}{L_{bat2}} e_{02} \quad (3.73)$$

$$\dot{v}_{c1,B} = -\frac{1}{R_{01}C_{01}}\, v_{c1,B} + \frac{1}{C_{01}} i_{bat1}, \dot{v}_{c2,B} = -\frac{1}{R_{02}C_{02}}\, v_{c2,B} + \frac{1}{C_{02}} i_{bat2} \quad (3.74)$$

where, d_{bat1} and d_{bat2} are the battery duty ratios determined by its droop mechanism in (3.88).

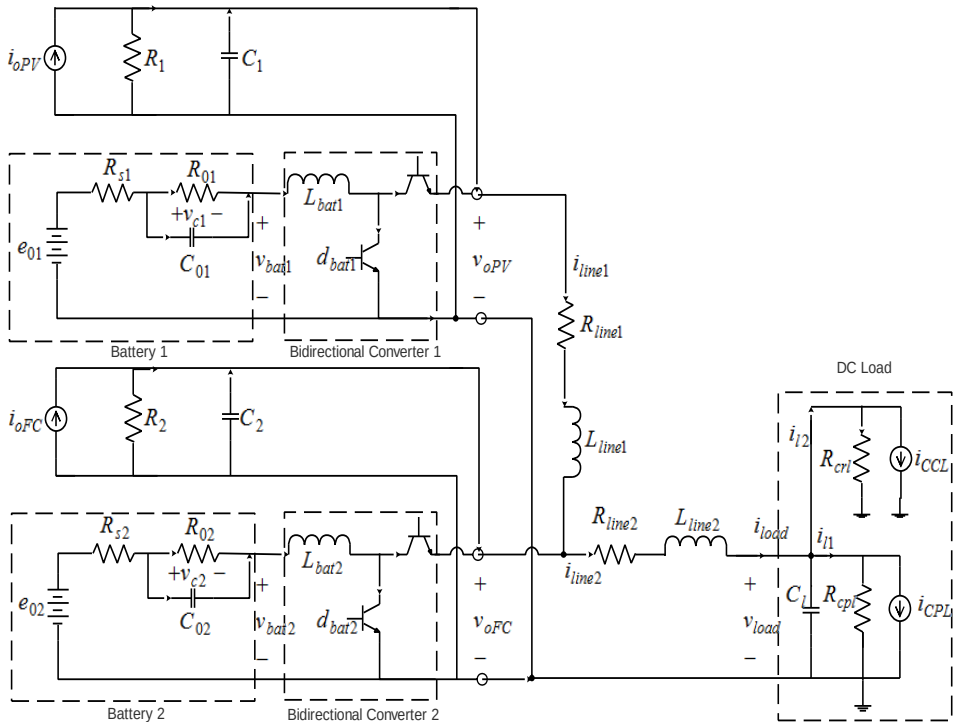

Figure 3.18. *Circuit diagram of DC microgrid interconnections.*

3.3.2.4 Load and Line Model

The equivalent load dynamics consists of two parallel load combinations of constant power load and constant voltage load. The linearized model of constant power load consists of an equivalent negative resistance, R_{cpl} and equivalent current sink,i_{CPL}. A combination of equivalent resistance of constant resistance load, R_{crl} and equivalent current sink representing constant current load forms another set of generalized load model. The total load current i_{load} is the sum of current in both parallel branches as follows.

$$i_{load} = i_{l1} + i_{l2} = \left(i_{cl} + i_{CPL} + \frac{v_{load}}{R_{cpl}}\right) + \left(i_{CCL} + \frac{v_{load}}{R_{crl}}\right) = i_{cl} + i_{cc} + \frac{v_{load}}{R_{cc}} \quad (3.75)$$

where, $i_{cc} = i_{CPL} + i_{CCL}$ and $R_{cc} = \frac{R_{cpl}R_{crl}}{R_{cpl}+R_{crl}}$

The state equation derived by the load dynamics is given in (3.76), where i_{cc} represents the load current sink and R_{cc} represents the total resistive load.

$$\dot{v}_{load} = \frac{1}{C_l}\left(i_{load} - i_{cc} - \frac{v_{load}}{R_{cc}}\right) \tag{3.76}$$

The equivalent model of lumped π-type connecting cable consists of series combination of line resistance and line inductance. Considering separate connecting cables between the two sources and fuel cell-load module as in Figure 3.18., the load current states are evaluated in (3.77).

$$\begin{aligned} i_{line1} &= -\frac{R_{line1}}{L_{line1}} i_{line1} + \frac{1}{L_{line1}} v_{oPV} - \frac{1}{L_{line1}} v_{oFC} \\ i_{line2} &= -\frac{R_{line2}}{L_{line2}} i_{line2} + \frac{1}{L_{line2}} v_{oFC} - \frac{1}{L_{line2}} v_{load} \end{aligned} \tag{3.77}$$

where, R_{line1}, L_{line1} and R_{line2}, L_{line2} are the resistance and inductance of the two lines respectively, and v_{load} is the voltage at the load terminal.

3.3.3 Control scheme for duty ratio regulation

The control scheme for a DC microgrid can be divided into three parts: first, a modified droop controller to regulate converter duty cycle such that the output voltage of converter varies inversely with current with the enhanced property of increased current sharing accuracy and output voltage restoration.

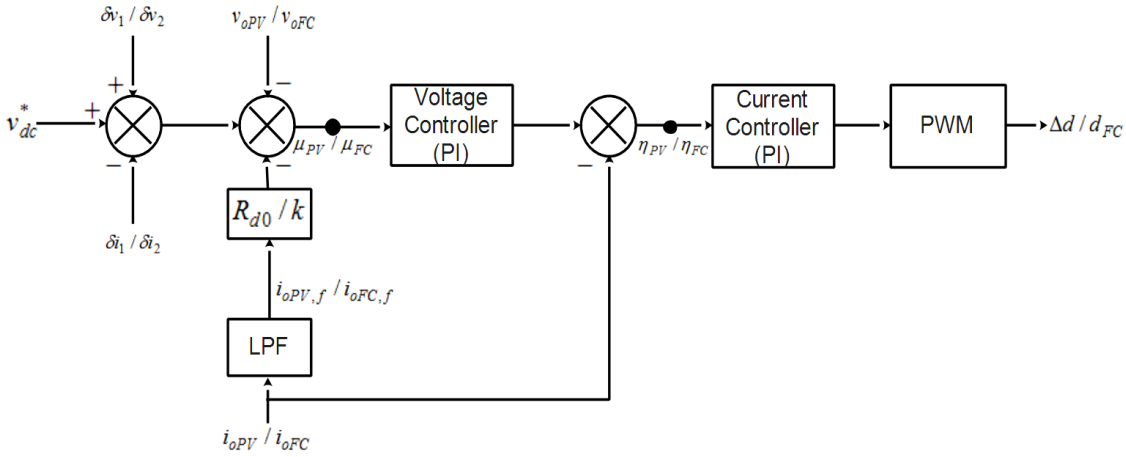

Figure 3.19. *Droop control mechanism.*

Second, power balancing droop controller for decentralized control of individual storage devices associated to different sources. Third, a linearized MPPT controller is mathematically obtained for maximum power point tracking in PV panel.

3.3.3.1 Droop control of photovoltaic and fuel cell converter

The two-faced control owing to primary and secondary level control hierarchy has been incorporated for steady state voltage and current control in DC microgrid through inclusion of a virtual resistance and current-voltage correction terms in system modelling as in Figure 3.19.

Primary control is achieved through an inner control loop which linearly decreases the output converter voltages as current increases. The general droop control is expressed as;

$$v_{o,i} = v_{dc}^* - R_{d,i} i_{o,i} \tag{3.78}$$

where, $v_{o,i}$ and $i_{o,i}$ is the output voltage and current of converter 'i' respectively; and v_{dc}^{*} is the reference value of dc output voltage and $R_{d,i}$ is the virtual resistance representing the droop characteristics.

Secondary control is achieved by correction term δi_1 and δv_1 which compensates for the voltage deviation and current degradation caused by droop mechanism. The reference DC voltage and averaged output converter voltage transmitted over a communication channel produces the voltage correction term, whereas the reference converter current output and averaged converter current generates the current correction term[27].

Droop control of PV-converter duty ratio

References [27-28] gives a detailed theoretical analysis of converter droop controller based on enhanced low-bandwidth communication. A mathematical formulation following the basic convention of considering the output of accumulator as a state variables, the droop based voltage and current correction terms has been obtained in equation (3.79).

$$\delta v_1 = k_{pv}\left(v_{dc}^{*} - \frac{v_{oPV}+G_d v_{oFC}}{2}\right) + k_{iv} g_{v.pv}$$

$$\delta i_1 = k_{pc}\left(\frac{i_{oPV}}{k_1} - \frac{i_{oPV}/k_1 + G_d i_{oFC}/k_2}{2}\right) + k_{ic} g_{c.pv} \tag{3.79}$$

where, k_{pv}, k_{iv}; k_{pc}, k_{ic} are the PI gains of voltage and current average controllers. k_1 and k_2 denote the percentage current sharing by the two converters. (let, $k_1 = k_2 = 1$)

Considering negligible latency in communication link, the state equations of average voltage and current controllers are (3.80-3.81). Assuming a LPF with cut-off

frequency ω_c rad/sec for the converter output current in droop control loop and two subsequent accumulator outputs μ_{pv} and η_{pv} as state variables, the state equations are:

$$\dot{g}_{c,pv} = \frac{i_{oPV}}{k_1} - \frac{i_{oPV}/k_1 + G_d i_{oFC}/k_2}{2}$$

$$\dot{g}_{v,pv} = v_{dc}^* - \frac{v_{oPV} + G_d v_{oFC}}{2} \tag{3.80}$$

$$\dot{i}_{opv,f} = -\omega_c i_{opv,f} + \omega_c i_{oPV}$$

$$\dot{\mu}_{pv} = v_{dc}^* + \delta v_1 - \delta i_1 - \frac{R_{d0}}{k_1} i_{opv,f} - v_{oPV}$$

$$\dot{\eta}_{pv} = k_{pvl}\dot{\mu}_{pv} + k_{ivl}\mu_{pv} - i_{oPV} \tag{3.81}$$

where, k_{pvl}, k_{ivl} are PI gains of voltage loop; R_{d0} is the constant virtual resistance reflecting droop characteristics.

The duty cycle ratio is obtained as the normalized droop output pulses;

$$\Delta d = k_{pcl}\frac{\dot{\eta}_{pv}}{v_{oPV}} + k_{icl}\frac{\eta_{pv}}{v_{oPV}} \tag{3.82}$$

where, k_{pcl}, k_{icl} are PI gains of current loop.

Droop control of fuel cell-converter duty ratio

The duty cycle ratio, d_{fc}, given as normalized output pulses to drive the fuel cell converter system can be derived from a set of mathematical equations for fuel cell-converter droop control in (3.83-3.85).

$$\delta v_2 = k_{pv}\left(v_{dc}^* - \frac{v_{oFC} + G_d v_{oPV}}{2}\right) + k_{iv} g_{v,fc}$$

$$\delta i_2 = k_{pc}\left(\frac{i_{oFC}}{k_2} - \frac{i_{oPV}/k_1 + G_d i_{oFC}/k_2}{2}\right) + k_{ic} g_{c,fc} \tag{3.83}$$

$$\dot{g}_{v,fc} = v_{dc}^* - \frac{v_{oFC} + G_d v_{oPV}}{2}$$

$$\dot{g}_{c,fc} = \frac{i_{oFC}}{k_2} - \frac{i_{oFC}/k_2 + G_d i_{oPV}/k_1}{2} \tag{3.84}$$

$$\dot{i}_{ofc,f} = -\omega_c i_{ofc,f} + \omega_c i_{oFC}$$

$$\dot{\mu}_{fc} = v_{dc}^{*} + \delta v_2 - \delta i_2 - \frac{R_{d0}}{k_2} i_{ofc,f} - v_{oFC}$$

$$\dot{\eta}_{fc} = k_{pvl}\dot{\mu}_{fc} + k_{ivl}\mu_{fc} - i_{oFC} \tag{3.85}$$

$$d_{fc} = k_{pcl}\frac{\dot{\eta}_{fc}}{v_{oFC}} + k_{icl}\frac{\eta_{fc}}{v_{oFC}} \tag{3.86}$$

where, all the PI gains are same as that for PV system for sake of simplicity.

3.3.3.2 Droop control of battery

The reference [25] derives a battery reference current from a slower outer loop based on P-V droop characteristics so as to balance power requirements. To keep the focus of this study on the time separation based on fuel cell dynamics, this slower outer loop has been ignored by considering the reference battery currents, $i_{bat1}^{*}$and i_{bat2}^{*} as inputs to the overall state space model. The two state equations and duty ratios d_{bat1}, d_{bat2} are given in (3.87-3.88).

$$\dot{z_1} = i_{bat1} - i_{bat1}^{*} - k_{f1}z_1$$

$$\dot{z_2} = i_{bat2} - i_{bat2}^{*} - k_{f2}z_2 \tag{3.87}$$

$$d_{bat1} = k_{pc}\frac{(i_{bat1} - i_{bat1}^{*})}{v_{oPV}} + k_{ic}\frac{z_1}{v_{oPV}}$$

$$d_{bat2} = k_{pc}\frac{(i_{bat2} - i_{bat2}^{*})}{v_{oFC}} + k_{ic}\frac{z_2}{v_{oFC}} \tag{3.88}$$

where, k_{pc} and k_{ic} are the PI gains of current controller.

3.3.3.3 MPPT control

The objective of Maximum Power Point Tracking (MPPT) controller is to track the Maximum Power Point(MPP) of the PV source. The mathematical model of a fast MPPT

controller to regulate the duty cycle of PV connected converter system is obtained from [29]. The controller is basically follows a PI control strategy wherein input is the value of dP_{PV}/dV_{PV}. Thus the linearized expression for derived duty cycle is given in (3.88) and the state variable, $\emptyset_{pv}$, represents the cumulative perturbations in PV current as in (3.89).

$$\widetilde{d(t)} = k_{p,mpp} G_{pv} i_{pv} + k_{i,mpp} G_{pv} \emptyset_{pv} \tag{3.89}$$

$$\dot{\emptyset}_{pv} = i_{pv} \tag{3.90}$$

where, $G_{pv} = \left.\frac{\partial(dP_{PV}/dV_{PV})}{\partial i_{pv}}\right|_{i_{pv}=I_{PV}}$ is considered to be a constant value. The droop-MPPT controller regulating the duty cycle of PV-converter system works in two modes given by two cases as;

$$d_{pv} = \begin{cases} \widetilde{d(t)} & MPPT\ mode \\ \widetilde{d(t)} + \Delta d & MPPT + Droop\ mode \end{cases} = \begin{cases} d_1 & MPPT\ mode \\ d_2 & MPPT + Droop\ mode \end{cases} \tag{3.91}$$

3.3.4 State Space Representation of DC Microgrid System

The overall nonlinear state space model consisting of system components and control strategies is derived by substituting the duty ratios d_{pv}, d_{fc}, d_{bat1} and d_{bat2} in (3.86), (3.88), (3.91) derived from respective controller blocks into the converter state equations (3.70), (3.72) and (3.73) such that the individual states are combined as;

$$\boldsymbol{x} = [\boldsymbol{x_{fc}}\ x_{opv}\ x_{ofc}\ \boldsymbol{x_{pv,conv}}\ \boldsymbol{x_{fc,conv}}\ x_{mppt}\ \boldsymbol{x_{droop,pv}}\ \boldsymbol{x_{droop,fc}}\ \boldsymbol{x_{bat}}\boldsymbol{x_{droop,bat}}\ \boldsymbol{x_{line}}\ \boldsymbol{x_{load}}]^{\boldsymbol{T}} \tag{3.92}$$

where, $\boldsymbol{x_{pv,conv}} = [i_{L,PV}\ v_{c1,PV}\ \ v_{c2,PV}]$ $\quad$,$\boldsymbol{x_{fc,conv}} = \left[\ x_{fc}\ i_{L,FC}\ v_{c,FC}\right]$, $\quad x_{mppt} = \emptyset_{pv}$, $\boldsymbol{x_{bat}} = [i_{bat1}\ i_{bat2}\ v_{c1,B}\ v_{c2,B}]$, $\boldsymbol{x_{droop,bat}} = [z_1\ z_2]$, $\boldsymbol{x_{line}} = [i_{line1}\ i_{line2}]$ and $x_{load} = v_{load}$ as obtained in (3.76).

The PV and fuel cell-converter output voltages derived with reference to network dynamics as in Figure 3.18., is given in (3.93).

$$\dot{x}_{oPV} = \dot{v}_{oPV} = \frac{a_1}{c_1}\ i_{oPV} + \frac{1}{C_1}\ d_{bat1} i_{bat1} - \frac{1}{C_1} i_{line1} - \frac{1}{R_1 C_1}\ v_{oPV}$$

$$\dot{x}_{oFC} = \dot{v}_{oFC} = \frac{a_2}{c_2}\ i_{oFC} + \frac{1}{c_2} d_{bat2}\ i_{bat2} + \frac{1}{c_2} i_{line1} - \frac{1}{c_2} i_{load} - \frac{1}{R_2 C_2}\ v_{oFC} \tag{3.93}$$

where, a_1 and a_2 represents the portion of source power delivered to the microgrid under stable operating conditions for PV and fuel cell respectively.

The nonlinear state space model of the full order DC microgrid is represented as;

$$\dot{\boldsymbol{x}} = \boldsymbol{f}(\boldsymbol{x}, \boldsymbol{u}, \boldsymbol{w})$$

$$y = v_{load} = \boldsymbol{C}\boldsymbol{x} \tag{3.94}$$

where, State variables;

$$\boldsymbol{x} = [(m_{O_2})_{net}; (m_{H_2})_{net}; (m_{H_2O})_{net}; T; P_{H_2}; P_{O_2}; P_{H_2O}; Q_C; Q_E; Q_L; v_{cd}; v_{oPV}; v_{oFC}; i_{L,PV}; v_{c1,PV}; v_{c2,PV}; i_{L,FC}; v_{c,FC}; \emptyset_{pv}; i_{opv,f}; \mu_{pv}; \eta_{pv}; g_{v.pv}; g_{c.pv}; i_{ofc,f}; \mu_{fc}; \eta_{fc}; g_{v.fc}; g_{c.fc}; i_{bat1}; i_{bat2}; v_{c1,B}; v_{c2,B}; z_1; z_2; i_{line1}; i_{line2}; v_{load}] \tag{3.95}$$

Control input, $\boldsymbol{u} = [u_{P_A} u_{P_C} u_{T_R} v_{PV} v_{FC}\ i_{oPV} i_{oFC} v_{dc}^* i_{bat1}^* i_{bat2}^* e_{01} e_{02} i_{cc}]^T$

Disturbance input, $\boldsymbol{w} = [I]$

$\boldsymbol{C} = [0_{1\times 37}\ 1]$ with dimensionality 1×38; dimensionality of x, u and w are 38×1;13×1 and 1×1 respectively.

Thus this section determines the state space representation of the microgrid systems by mathematical modelling of the individual components and control schemes in a cumulative manner.

3.4 Simulation Results

The simulation results of the small signal modelling of microgrid system on MATLAB/SIMULINK 2016a on Intel(R) Core™ i5-5200U CPU 2.20GHz (4.00 GB RAM) are given in this section.

The complete small signal modeling of an autonomous AC microgrid, considering a small perturbation of ΔA on the state matrix A linearized in the vicinity of a steady state operating point, consisting of two DERs, local loads and a connecting line is represented in state space by state space equations and output equations as in (3.43-3.44). The PLL angular frequency profile for perturbed and unperturbed microgrid system in terms of two operating points is given in Figure 3.20. The effect of state perturbations on autonomous micro grid system dynamics can be seen in Figure 3.21.

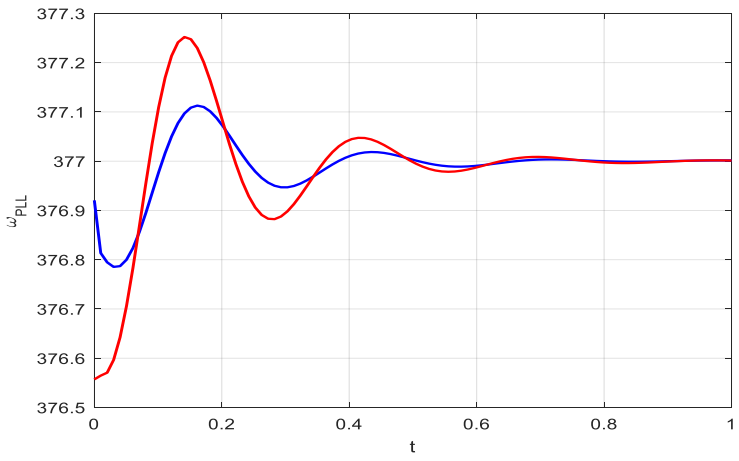

Figure 3.20. *Measured frequency by PLL.*

(blue and red color denotes operating points X_{oper1} and X_{oper2}, respectively)

The dynamical response of v_{odq} and i_{odq} of the system with and without perturbation, are shown in Figure 3.21.(c) and 3.21.(d). It is worthy to mention that the effect of perturbation on output voltage and current profile almost tracks with little deviation in the initial period due to certain system uncertainties. After 0.5 second the tracking error is almost zero. Similar case is also visualized corresponding to other system behavioral quantities. Here convergence is almost achieved even earlier in the initial period.

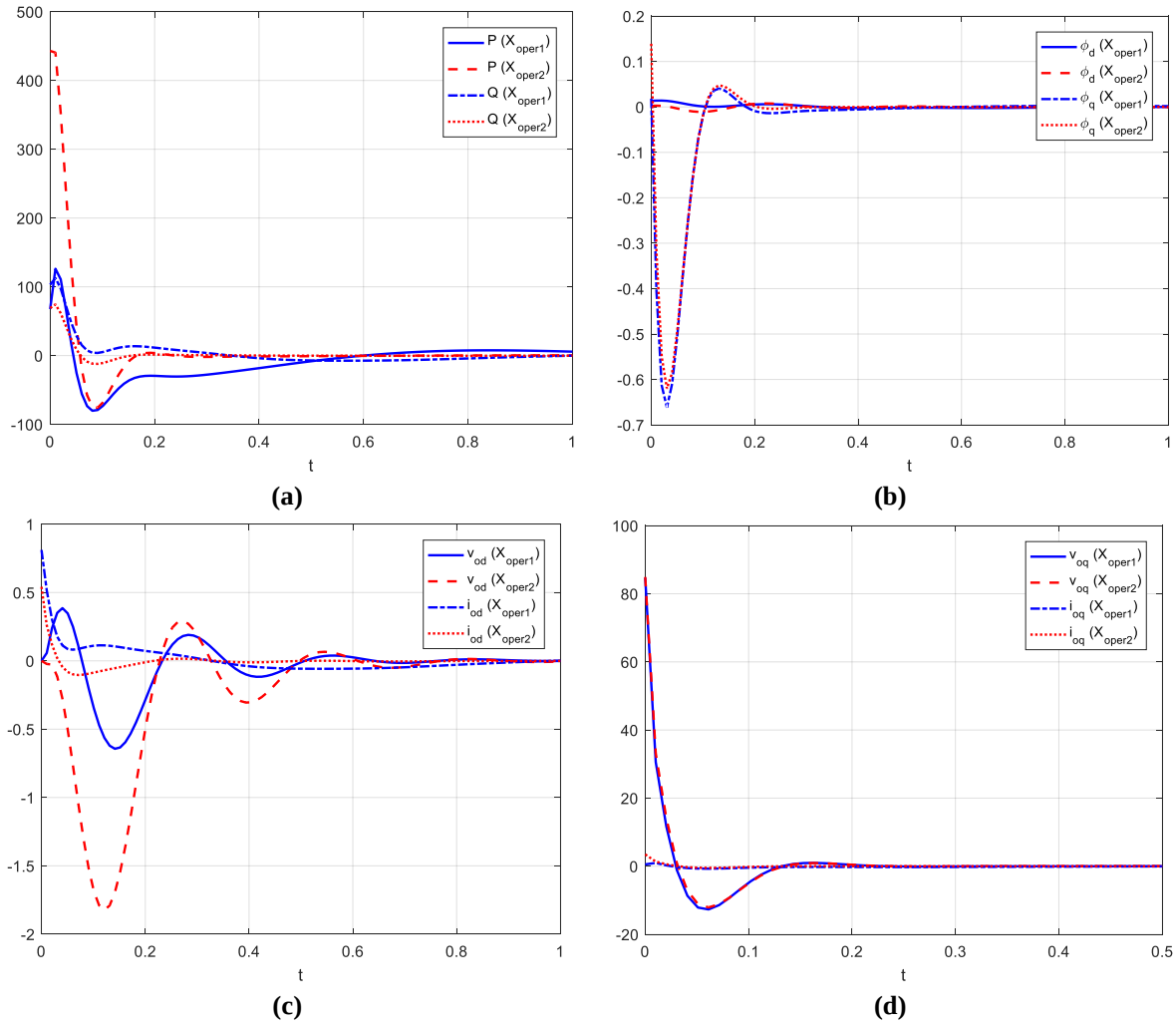

Figure 3.21*. Autonomous Microgrid System Profile (blue line indicates unperturbed system and red line indicates perturbed system) (a) Active and reactive power, (b)* φ_d, φ_q *(c) d-axis output current and voltage, (d) q-axis output current and voltage.*

Table 3.1. Eigenvalues obtained in different cases in grid-tied AC microgrid model.

	Eigenvalues			
Eigenvalue indices	***Case 1*** *Unperturbed system*	***Case 2*** *Uncertainty due to oscillations in LPF cut-off frequencies (1%)*	***Case 3*** *Uncertainty in measured powers at the steady state (0.2%)*	***Case 4*** *Uncertainty in measured powers at the steady state (-0.05%)*
1	0	0	0	0
2,3	-3999.1639 ±11.1381i	-3999.1639 ±11.1381e3i	-3999.1639 ±11.1381e03i	-3999.1639 ±11.1381e03i
4	-8397.4010	-8397.4011	-8397.4011	-8397.4011
5,6	-765.6479 ±11320.5331i	-765.6480 ±11320.5332i	-765.6480 ±11320.5332i	-765.6480 ±11320.5332i
7	-462.0381	-462.0382	-462.0381	-462.0386
8	-391.4367	-391.4360	-391.4360	-391.4368
9	-54.6187	-54.6091	-54.6092	-54.6201
10	-45.0823	-45.0798	-45.0798	-45.0827
11	-50.2610	-50.2620	-50.2620	-50.2599
12	-50.2602	-50.2716	-50.2716	-50.2594
13	-1.6376	-1.6373	-1.6373	-1.6375
14	-32.0808×10^{-6}	-188.2018×10^{-6}	-187.4150×10^{-6}	18.8672×10^{-6}
15	-16.1113×10^{-6}	-374.6750×10^{-6}	-373.1089×10^{-6}	9.4749×10^{-6}

Further, for the small signal model of grid-tied microgrid system as in (3.67) a detailed state perturbation analysis has been carried out in the form of eigenvalues and system dynamics in Table 3.1. Four different cases with definite changes in the system parameters in the form of percentage values has been considered and their impact on the location of eigenvalues has been analyzed. Their subsequent dynamical changes has also been studied graphically.

The perturbation in the state space model due to various reasons discussed in Section 3.1 lead to deviations in the system dynamics. Uncontrolled perturbations need

to be monitored in order to ensure system stability in all operating conditions. A case study of some of the perturbations in the microgrid model, given in Table 3.1, are considered in this work to demonstrate their effects on system stability which will be analysed in Chapter 5.

Figure 3.22., demonstrates the effect of different cases under consideration on the system dynamics. The overlapping PLL frequency waveforms in Figure 3.22.(e) for all the four cases depict the efficient small signal modelling for the microgrid systems.

3.5 Summary

In this chapter, the AC and DC microgrid architectures considered in this thesis has been mathematically modelled. However, the small signal analysis of the AC microgrid systems in this chapter develops a 36^{th} order state space model of droop-controlled model in autonomous mode and 15^{th} order state space model in grid-tied mode. A 38^{th} order PV-fuel cell DC microgrid in autonomous mode has also been modelled to demonstrate the system dynamics with both droop controller and MPPT controller. Simulation results for the state space system dynamics with the impact of state perturbations also been included.

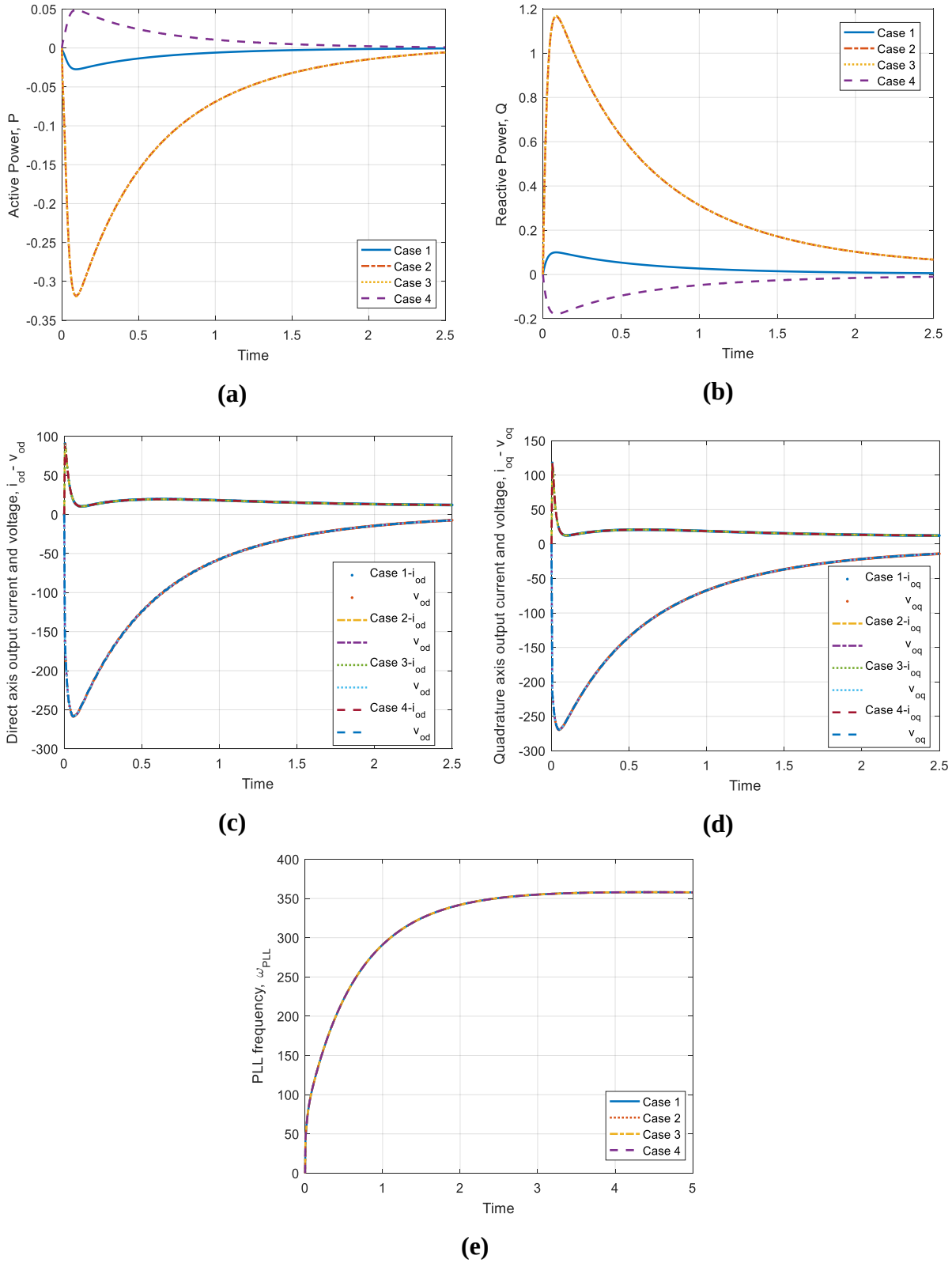

Figure 3.22. *Grid-tied Microgrid System Profile: (a)Active power, (b)Reactive power, (c)Direct axis output current and voltage, (d)Quadrature axis output current and voltage, (e)PLL frequency.*